Chapter 5

Synthesis, Atomic Structures and Properties of Boron Nitride Nanotubes

Takeo Oku

Additional information is available at the end of the chapter

http://dx.doi.org/10.5772/51968

1. Introduction

Since the development of boron nitride (BN) nanotubes (Chopra et al. 1995), various types of BN nanostructured materials have been reported because of the great potential for using materials with low dimensions in an isolated environment. Many studies have been reported on BN nanomaterials and single crystals such as nanotubes (Golberg et al. 2000, Mickelson et al. 2003), bundled tubes, nanocorns, nanohorns, nanocapsules, nanoparticles, BN clusters, and BN metallofullerenes, which are expected to be useful as electronic devices, field-effect transistors (Radosavljevi et al. 2003), high heat-resistant semiconductors, insulator lubricants, nanowires (Tang et al. 2002), magnetic nanoparticles, gas storage materials (Lim et al. 2007), and optoelectronic applications including ultraviolet light emitters. Theoretical calculations on BN nanomaterials such as nanotubes (Rubio et al. 1994), cluster-included nanotubes, BN clusters, BN metallofullerenes, cluster solids, nanohorns, and hydrogen storage have also been carried out for prediction of the properties. By controlling the size, layer numbers, helicity, compositions, and included clusters, these cluster-included BN nanocage structures with bandgap energy of ~6 eV (Watanabe et al. 2004) and nonmagnetism are expected to show various electronic, optical, and magnetic properties as shown in Fig. 1. The differences between BN and carbon nanomaterials (Oku et al. 2009) are summarized as shown in Table 1.

The present review shows BN nanotubes synthesized by arc melting and thermal annealing methods. They were characterized by high-resolution electron microscopy (HREM), and their properties were investigated and discussed. In order to confirm the atomic structures and to investigate stabilities and electronic states, total energy calculations were carried out by molecular mechanics and molecular orbital calculations. These studies will give us a guideline for the synthesis of the BN nanotubes, which are expected for the future nanoscale devices.

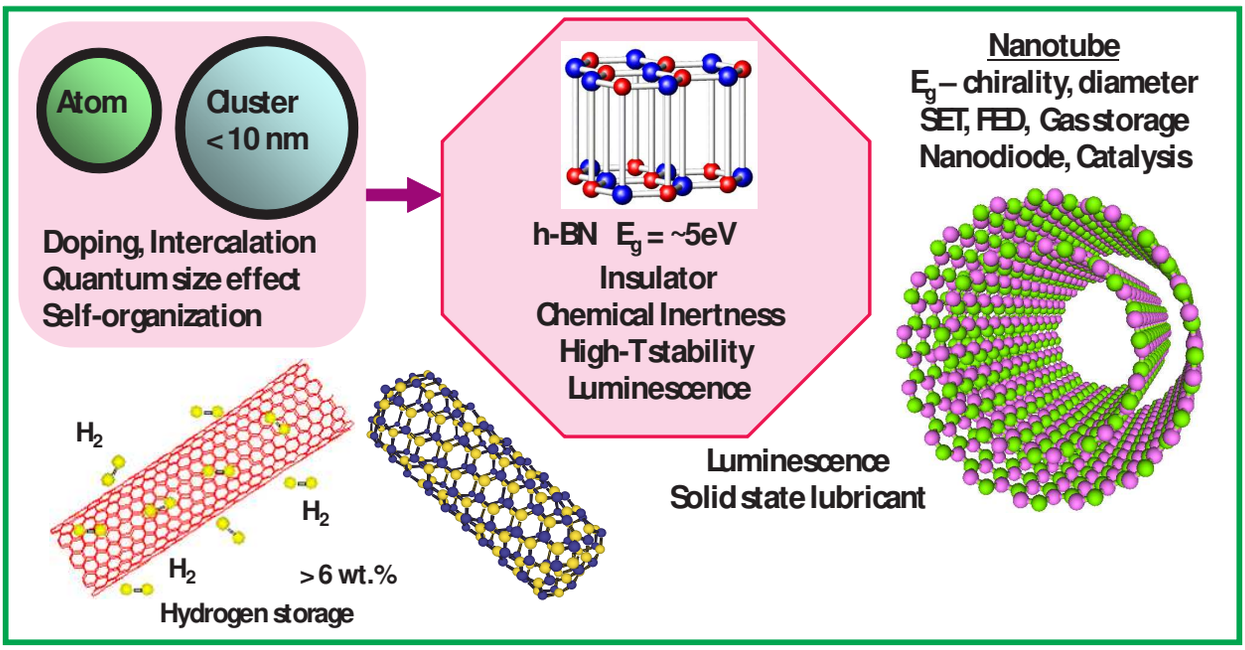

Figure 1. Structures and properties of BN nanotubes

	BN	C
Structure	4-, 6-, 8-membered rings	5-, 6-, 7-membered rings
Oxidation resistance	~900°C	~600 °C
Electronic property (E_g)	Insulator (~6 eV)	Metal-semiconductor (0~1.7 eV)
Band structure	Direct transition	Indirect transition

Table 1. Differences between BN and carbon (C) nanotubes

2. Synthesis of BN nanotubes

2.1. Arc-melting of boride powders

The purpose of the present work was to prepare the BN nanotubes by arc-melting YB_6 powder in nitrogen and argon gas atmosphere. Yttrium (Y) had been reported to show excellent catalytic properties for producing single-walled carbon nanotubes (Saito et al. 1995). In the present work, YB_6 was selected to take advantage of this excellent catalytic effect (Narita & Oku, 2003). It is not necessary to prepare the boride-rod if the YB_6 powder is used. To understand the formation mechanism of BN nanotubes, HREM and electron dispersive X-ray spectroscopy (EDX) were carried out.

The YB_6 powder (4.0 g, 99.6%, Kojundo Chemical Lab. Co., Ltd) was set on a copper mold in an electric-arc furnace, which was evacuated down to 1.0×10^{-3} Pa. After introducing a

http://dx.doi.org/10.5772/51968

mixed gas of Ar (0.025 MPa) and N_2 (0.025 MPa), arc-melting was applied to the samples at an accelerating voltage of 200 V and an arc current of 125 A for 10 s (. Arc-melting was performed with a vacuum arcmelting furnace (NEV-AD03, Nissin Engineering Co., Ltd). Samples for HREM observation were prepared by dispersing the materials on holey carbon grids. HREM observation was performed with a 300 kV electron microscope (JEM-3000F). To confirm the formation of BN fullerene materials, EDX analysis was performed by the EDAX system.

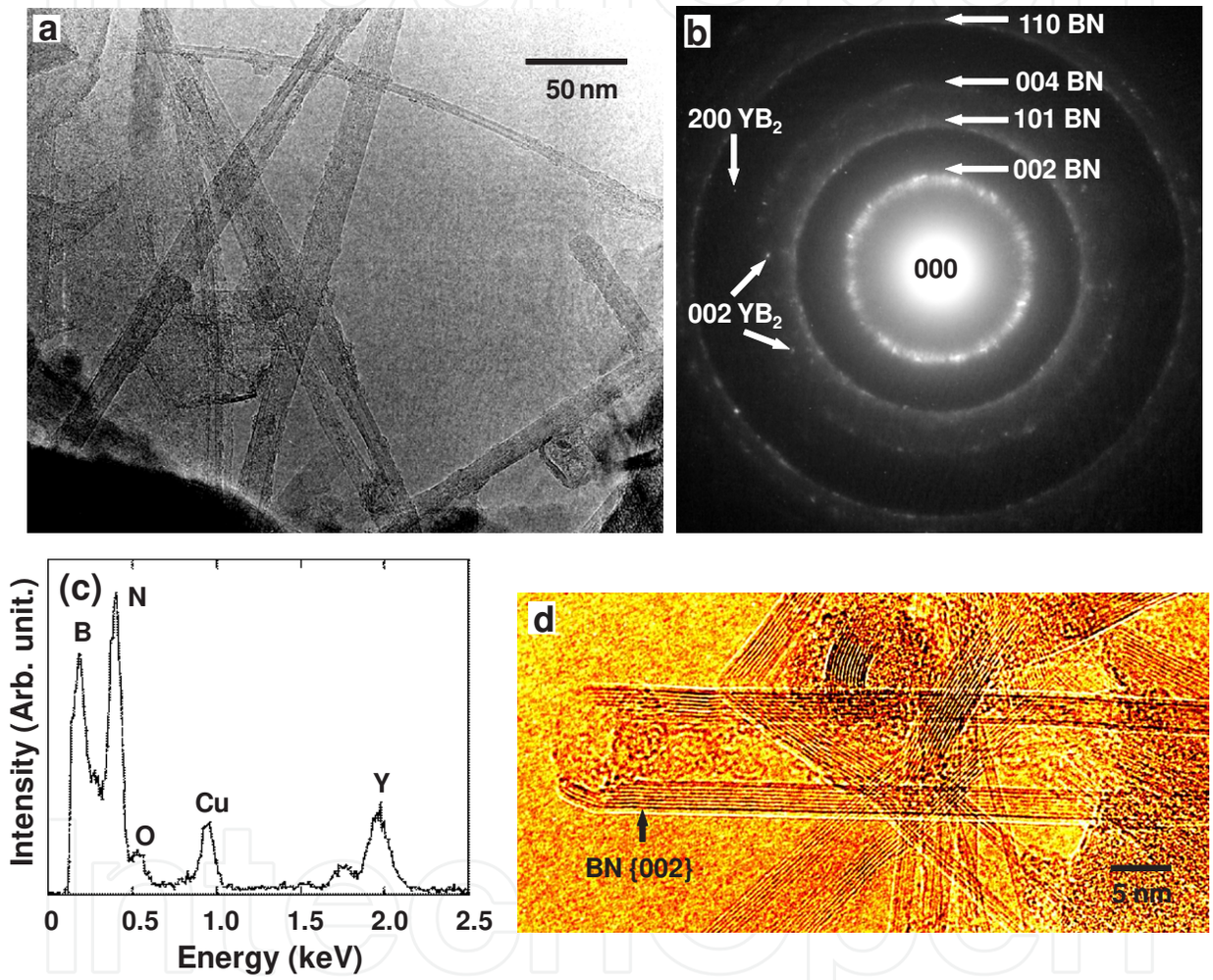

Figure 2. a) TEM image of BN nanotubes. (b) Electron diffraction pattern and (c) EDX spectrum of BN nanotubes with YB_x nanoparticles. (d) HREM images of BN nanotubes.

Low magnification image of BN nanotubes produced from YB_6 powder by arc-melting is shown in Fig. 2(a). In Fig. 2(a), length and width of the multi-wall BN nanotubes are in the range of 4–6 mm and 4–10 nm, respectively. An electron diffraction pattern of BN nanotubes with YBx nanoparticles indicate the existence of BN and YB_2, as shown in Fig. 2(b). In Fig. 2(a), {002} and {200} reflections of YB_2 are observed. Figure 2(c) is an EDX spectrum of BN nanotubes, and strong peak of boron, nitrogen, and Y are observed. Weak peak of copper is

due to the HREM grid. The EDX results showed the composition ratio of the BN nanotubes was B/N = 1.1:1. A HREM image of a multi-walled BN nanotube is shown in Fig. 2(d).

A HREM image of BN nanotube in Fig. 3(a) shows that the BN nanotube has asymmetry layer-arrangements. The layer interval on one side of the tube is 0.34 nm. Other side is in the range of 0.34–0.70 nm, which is larger than the {002} of ordinary hexagonal BN (0.34 nm). {100} planes of YB_2 are observed after the formation of BN nanotubes at the end of it, as shown in Fig. 3(b). Amorphous B with opened-tip BN nanotube is also formed at the same time by arc-melting YB_6 powder, as shown in Fig. 3(c). A novel BN nanotube is shown in Fig. 3(d). A wavy BN layer is formed into BN nanotube by most internal BN layers.

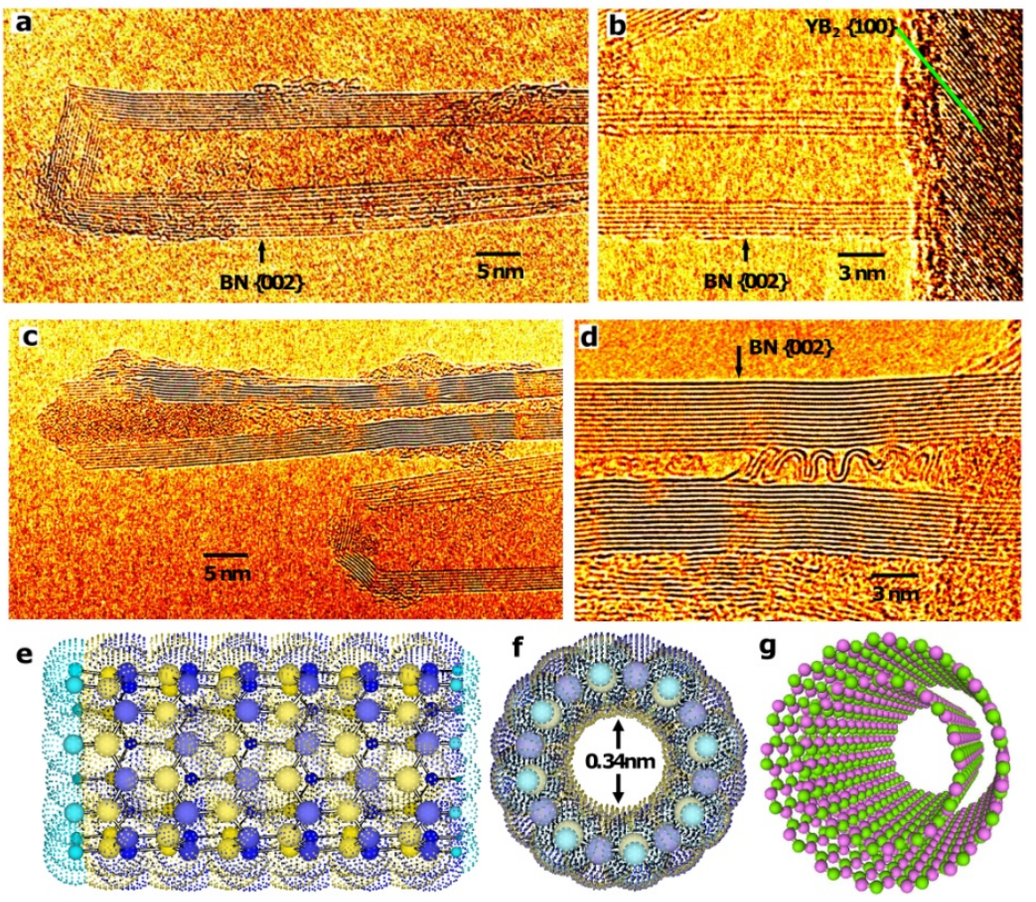

Figure 3. HREM images of (a) BN nanotube and (b) BN nanotube with YB_2 compounds. HREM images of (c) amorphous B with open-tip BN nanotube and (d) a wavy BN nanolayers in BN nanotube. Van der Waals force distribution in BN nanotube: (e) perpendicular to and (f) along the nanotube axis. Structure model of double-walled BN nanotube.

Figures 3(e) and 3(f) is a schematic illustration of Van der Waals force distribution of BN nanotube: (e) perpendicular to and (f) along the nanotube axis. The structure corresponds to the center of the BN nanotube. There is a space with a diameter of 0.34nm inside the BN nanotube, which would be expected to be a container for atomic storage. Figure 3(g) is an atomic structure model of double-walled BN nanotube.

	1/I	2/II	3	4	5	6	7	8	9	10	11	12	13/III	14/IV	15/V	16/VI	17/VII	18/VIII
1	H																	He
2	Li	Be											B ×	C	N	O	F	Ne
3	Na	Mg ×											Al ●	Si ×	P	S	Cl	Ar
4	K	Ca	Sc	Ti = ●	V ●	Cr	Mn	Fe ● =	Co ●	Ni ●	Cu ●	Zn	Ga ○	Ge ●	As	Se	Br	Kr
5	Rb	Sr	Y =	Zr =	Nb = ●	Mo	Tc	Ru	Rh	Pd ●	Ag	Cd	In	Sn	Sb	Te	I	Xe
6	Cs	Ba	La-Lu =	Hf =	Ta =	W =	Re	Os	Ir	Pt	Au ●	Hg	Tl	Pb	Bi	Po	At	Rn
7	Fr	Ra	Ac-Lr	Rf	Db	Sg	Bh	Hs	Mt									

Figure 4. Catalysis metals for BN fullerene nanomaterials confirmed by experiments on arc-method (=, BN nanotube; ●, BN nanocapsule; ○, BN nanocage; ×, non BN fullerene nanomaterials).

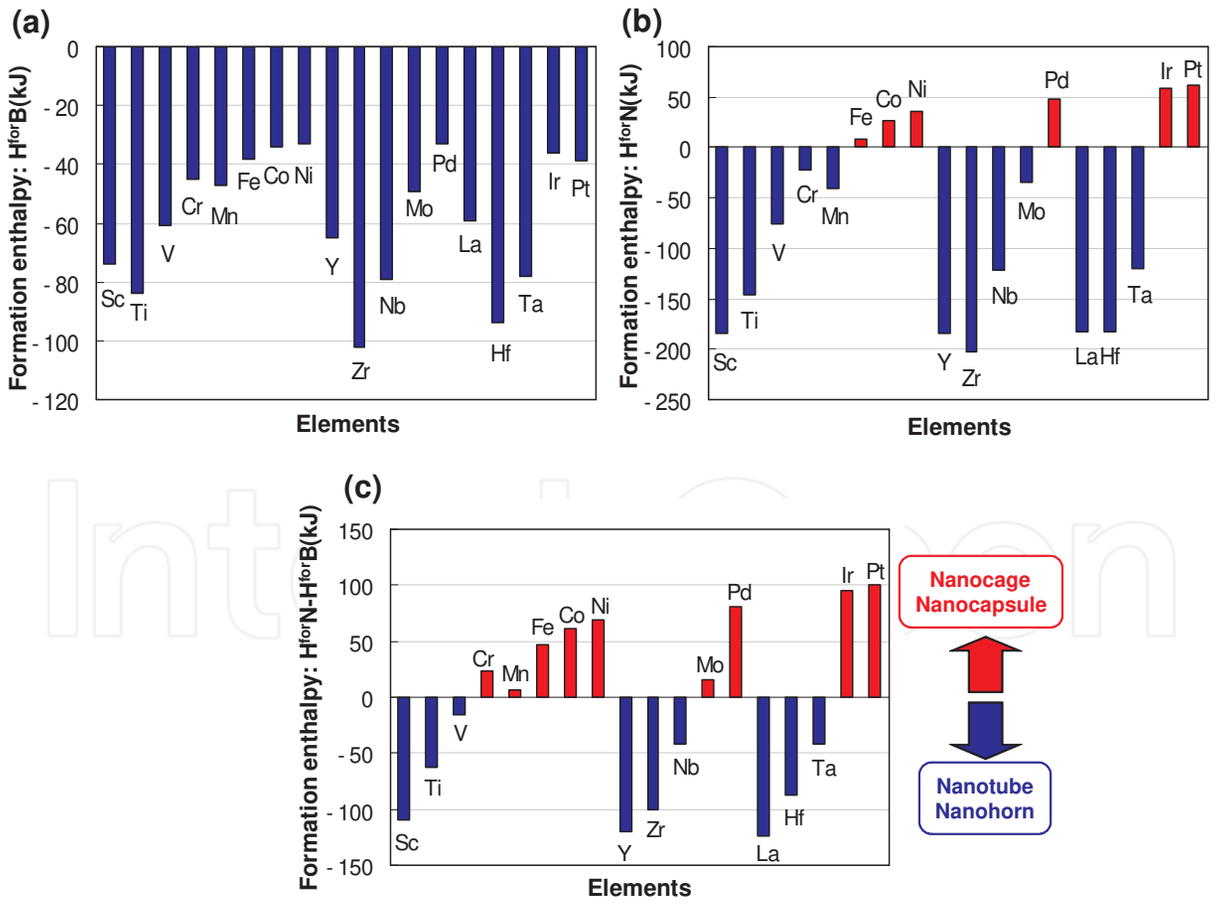

Figure 5. a) Formation enthalpy with boron ($H^{for}B$) and (b) nitrogen ($H^{for}N$); (c) Difference of formation enthalpy ($H^{for}N$ - $H^{for}B$).

In the present work, yttrium worked as a good catalytic element to produce BN nanotubes. Catalytic metals for the formation of BN nanotubes, nanocapsules, and nanocages, which were confirmed by experiments on arc method, are summarized in Fig. 4 as periodic table. It has been reported that Zr, Hf, Ta, W, Nb, and La can be good catalytic metals for synthesis of BN nanotubes (Narita et al. 2003). On the other hand, other metals could not form BN nanotubes, although BN nanocapsules or nanocages were formed.

For some metals, formation enthalpies with boron ($H^{for}B$) and nitrogen ($H^{for}N$) are indicated in Fig. 5(a) snf 5(b), respectively. The data were from theoretical calculations (Oku et al. 2004). Difference of formation enthalpy ($H^{for}N$ - $H^{for}B$) is also shown in Fig. 5(c). The difference of formation enthalpy ($H^{for}N$ - $H^{for}B$) is very important for the formation of BN fullerene nanomaterials. Because, reactivity with nitrogen and boron is decided by this enthalpy. Basically, BN nanotubes are formed when rare earth metals are used as catalytic metals, such as Y, Zr, Nb, Hf, Ta, W and La. These elements have minus enthalpy, as shown in Fig. 3c. It means that catalytic elements for synthesis of BN nanotubes should be selected from those with minus formation enthalpy ($H^{for}N$ - $H^{for}B$). From the present guideline, Sc element could be a good catalytic element to form BN nanotubes.

In the present work, the Y worked as a good catalytic element to produce BN nanotubes. Schematic illustration of the formation mechanism of BN nanotubes is shown in Fig. 6. First, ion and radical gas that consist of Y, B, and N elements would be produced by arc melting. This ion gas would be cooled by collision with Ar and N_2 gas. In this process, Y and B ions form particles of Y + B compound, which are semi-liquid state. Since B atoms become supersaturated on cooling, Y + B particles separate out B atoms on the surface. As a result, Y + B particles are covered with amorphous B. Some amorphous B would be separated from the surface of Y + B particles. BN nanolayers are formed between separated amorphous B and surface of Y + B particle. N that is necessary to form BN nanotube is provided from environmental gas. Also, B of Y + B particle would be used to form BN nanotube, because the YB_{6-x} compound is thermodynamically more stable than YB_6. In the present work, BN nanotubes with YB_2 particles are formed. Closed or opened tips of BN nanotubes would be formed by cooling rate. If enough time is not given to the formation of BN nanotubes, amorphous B with opened-tip BN nanotubes would be formed, as shown in Fig. 3(c).

Some of the multi-walled BN nanotubes have asymmetry layer-arrangements as shown Fig. 3(a) and 3(b). This asymmetry layer-arrangement comes from the difference of layer-arrangement of B and N atoms. In the case of hexagonal BN, B atoms infallibly exist just above the N atoms with the layer interval of 0.34 nm. However, in case of BN nanotube, some N atoms are close to the N atoms of other layers, because each BN layer of multi-walled BN nanotube has different diameter or chirality. In such case, since lone-pair of N atoms reacts against each other, BN layers have large layer interval at this part. On the other hand, a part that B atoms exist just above the N atoms keeps the layer interval of 0.34 nm. As a result, some BN nanotubes form asymmetry layer-arrangements.

http://dx.doi.org/10.5772/51968

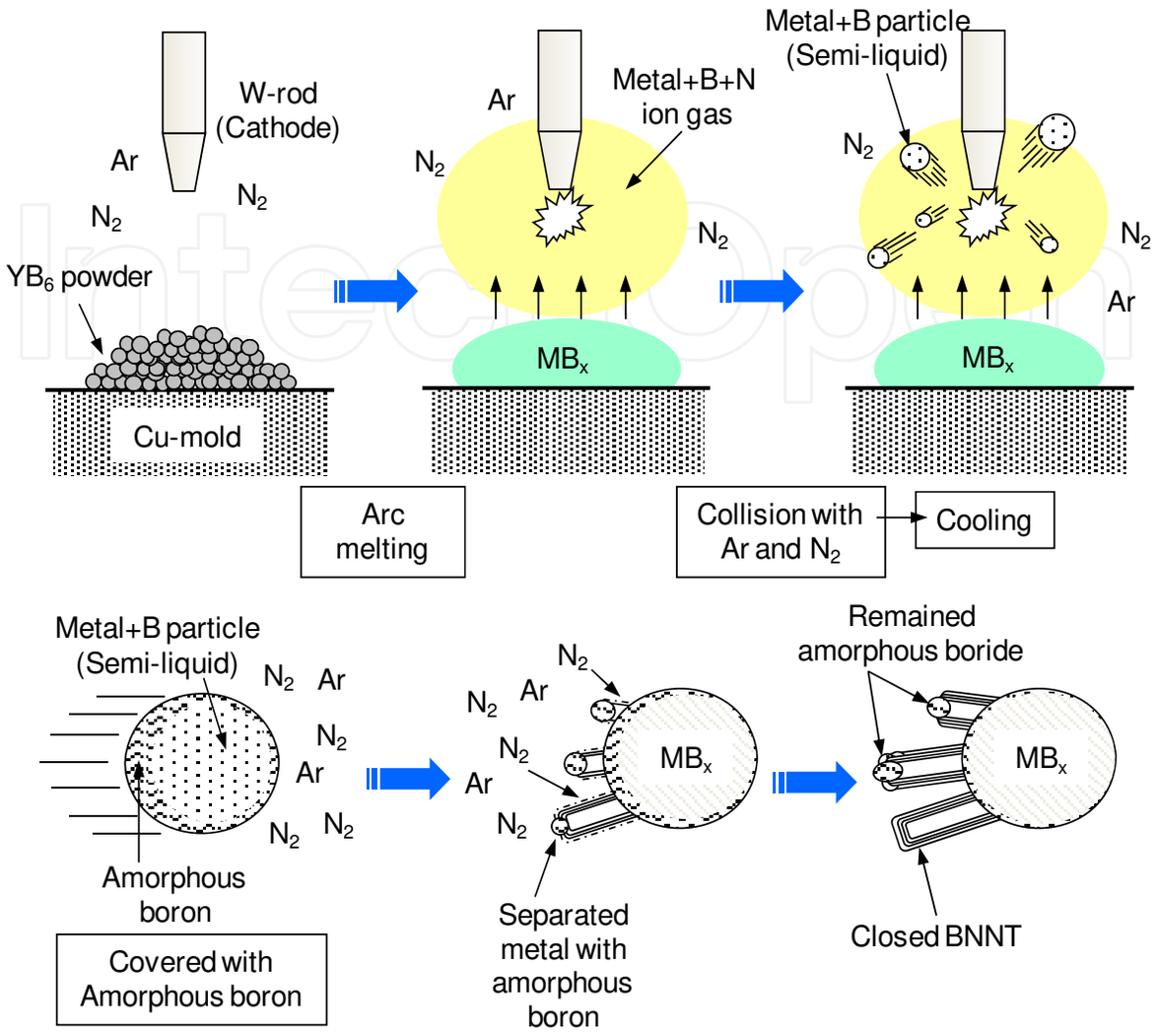

Figure 6. Schematic illustration of the formation mechanism of BN nanotubes.

2.2. Mass production of BN nanotubes

BN nanotubes have been synthesized by arc-discharge method, as decribed in the previous section. However, the arc-discharge method is not suitable for mass production because of limitation of the plasma area, and it is difficult to control nanotube size and the number of BN layers. The purpose is to synthesize BN nanotubes by ordinary thermal annealing, and to investigate the nanostructures. An Ellingham diagram of nitride metals for N_2 gas per mol was thermodynamically calculated by HSC Chemistry (Outokumpu Research Oy. Poli, Finland) software as shown in Fig. 7.

Fe_4N particles would be reduced to α-Fe completely by annealing with boron, because boron reacted with nitrogen more easily compared to Fe. Similarly, several nitrides would be reduced to pure metals by reaction with boron. In the present work, Fe was selected for the BN nanotube formation, and a mixture powder of Fe_4N/B was used for the synthesis (Koi et al. 2008).

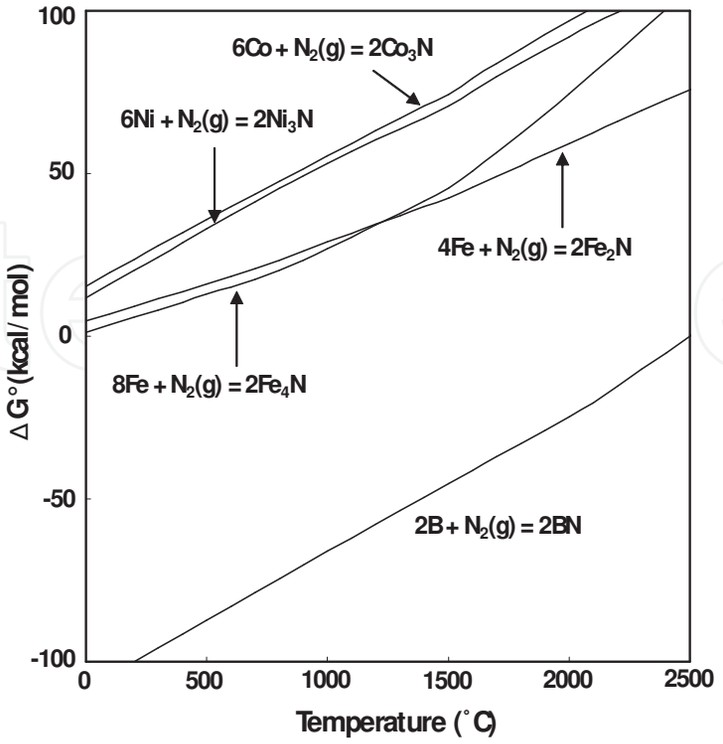

Figure 7. Ellingham diagram of Fe, Ni and Co nitrides for a N_2 molecule.

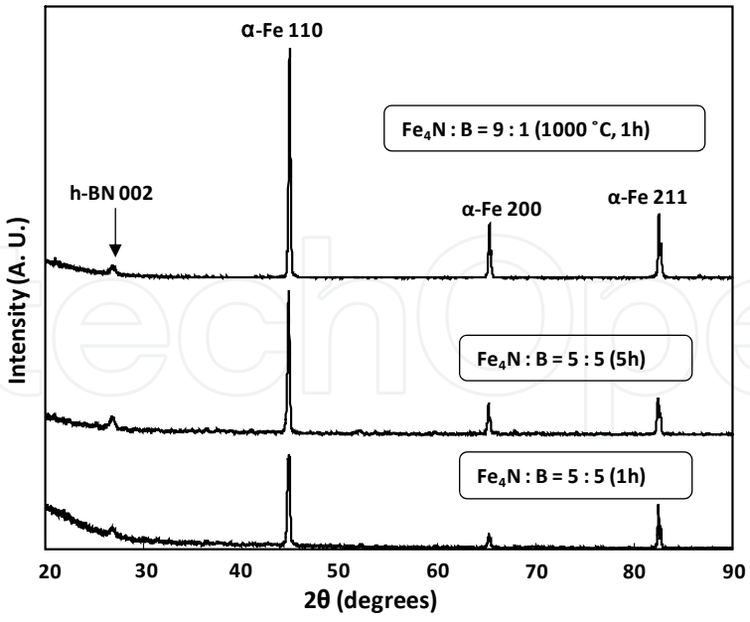

Figure 8. X-ray diffraction patterns of the annealed samples of Fe_4N:B, which are WR of Fe_4N:B = 5:5 annealed at 1000 °C for 1 h, (b) WR of Fe_4N:B = 5:5 annealed at 1000 °C for 5 h and (c) WR of Fe_4N:B = 9:1 annealed at 1000 °C for 1 h, respectively.

http://dx.doi.org/10.5772/51968

X-ray diffraction patterns of annealed samples of Fe_4N/B with various weight ratio (WR) of Fe_4N:B annealed at 1000 °C are shown in Fig. 8. Peaks of h-BN and α-Fe were confirmed for all samples, and no peak of Fe_4N and B was observed. Average diameters of Fe particles were measured to be 20~30 nm, which were calculated from halfwidths of α-Fe (110) by using the Scherrer's equation.

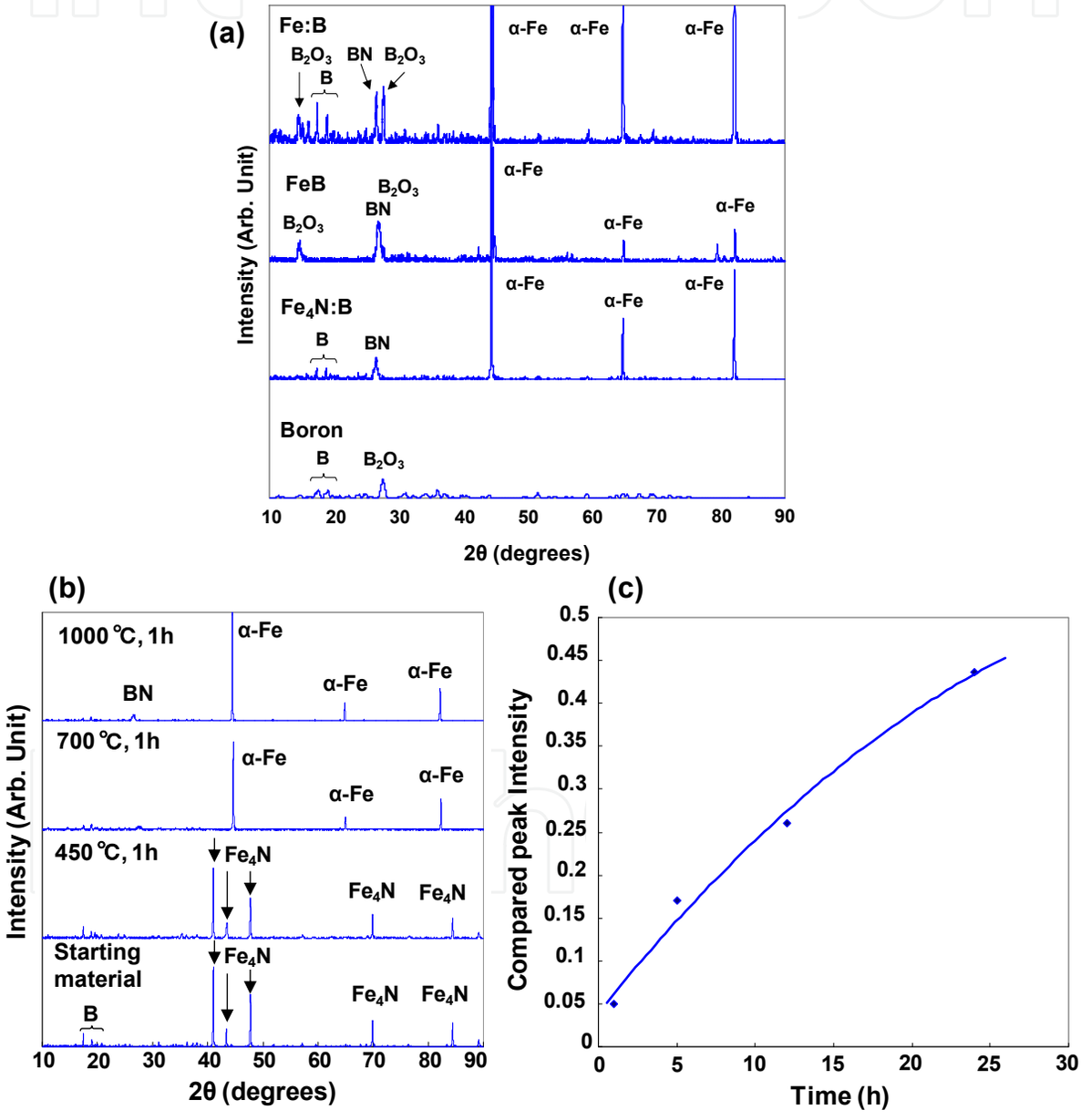

Figure 9. a) X-ray diffraction patterns of (a) various starting materials for BN nanotube formation after annealing at 1000 °C for 1 h. (b) X-ray diffraction patterns of samples at elevated temperatures. (c) Intensity change of BN as a function of annealing time. (=peak of BN/Fe)

To understand growth mechanism of BN nanomaterials, Fe_4N/B, Fe/B, FeB, B was used as starting materials, and the structures of BN nanomaterials were compared. Four-types of mixture powders (Fe/B, FeB, Fe_4N/B and B) were used as starting materials for BN synthesis. Particle sizes of Fe (purity of 99.5%, Mitsuwa's Pure Chemicals, Osaka, Japan), FeB (99%, Kojundo Chemical Laboratory (KCL) Co. Ltd., Saitama, Japan), Fe_4N (99.9%, KCL) and B (99%, KCL) were about 5, 850, 50, and 45 lm, respectively. After Fe/B and Fe_4N/B (Weight ratio [WR] = 1:1, respectively) were well mixed in a triturator, the samples were set on an alumina boat and annealed in the furnace. The furnace was programmed to heat at 6 °C /min from a room temperature to 450, 700, and 1000 °C and hold for 1–24 h, and then cooled at 3 °C /min to a room temperature. Nitrogen pressure was 0.10 MPa, and its gas flow was 100 sccm.

X-ray diffraction patterns of samples are shown in Fig. 9(a). Diffraction peaks of hexagonal BN and a-Fe were observed for each sample except for a sample synthesized from boron powder. Diffraction peaks of B_2O_3 were also observed for each sample except for a sample synthesized from Fe_4N/B powder. X-ray diffraction patterns of samples synthesized from Fe_4N/B were investigated at various temperatures and time. In Fig. 9(b), Fe_4N was reduced to Fe by boron at temperatures in the range of 450–700 °C, and BN was obtained at 1000 °C. Figure 9(c) shows intensity change of BN as a function of annealing time. A large amount of BN was obtained as time advances because Fe_4N would be sufficiently reduced to Fe.

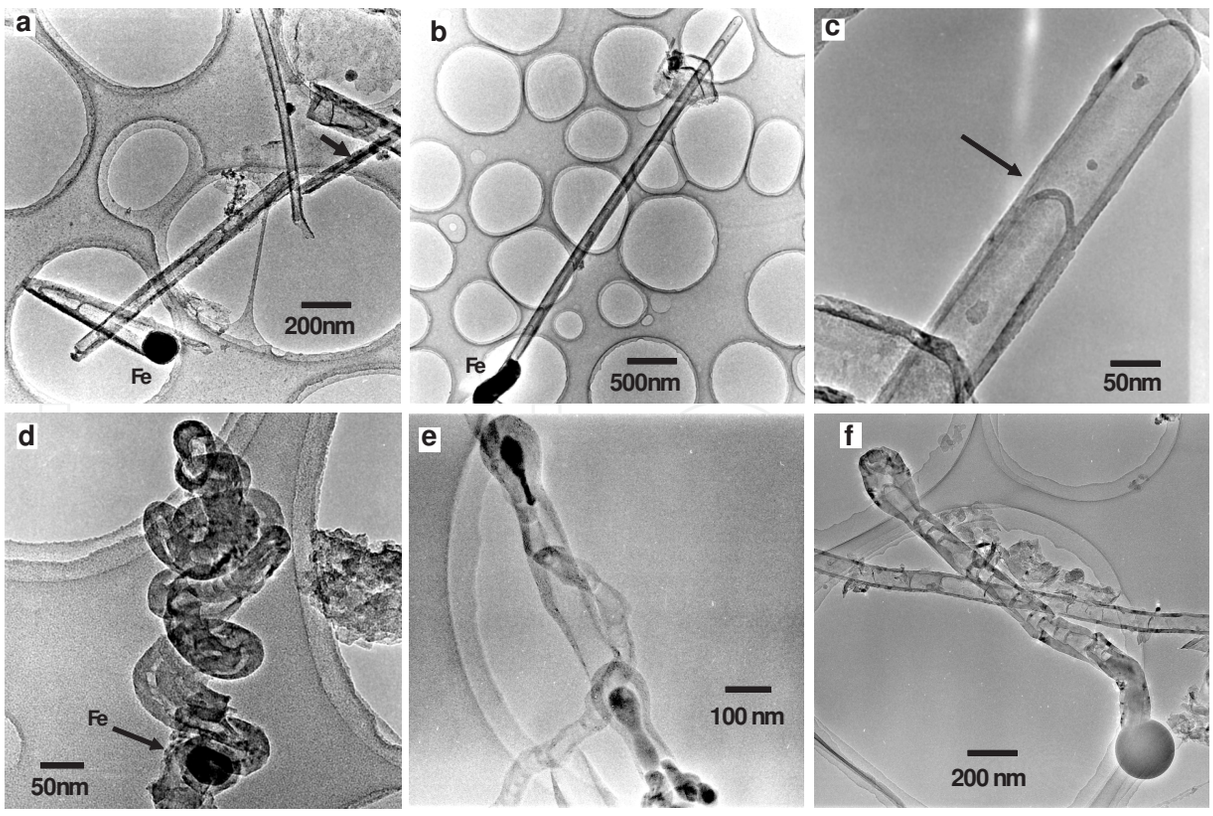

Figure 10. TEM images of BN nanotubes. (a) BN nanotubes and nanohorn. (b) BN nanotube with Fe nanoparticle. (c) Enlarged image of cap of (b). (d) BN nanocoil. (e) Bamboo-type BN nanotubes with Fe nanoparticles. (f) Bamboo-type nanotubes.

http://dx.doi.org/10.5772/51968

Phases of the samples were determined by X-ray diffraction, which showed peaks of hexagonal BN and α-Fe. Large amounts of BN nanotubes were produced, and Fig. 10(a) is a typical transmission electron microscope (TEM) image of the samples. BN nanohorn and nanotubes are observed, and lengths and widths of BN nanotubes were approximately 1–10 mm and 40–200 nm, respectively. A Fe nanoparticle is observed at the root area of a BN nanohorn. A nanotube shown by an arrow is a Fe-filled BN nanotube. Figure 10(b) is a TEM image of BN nanotube with a Fe nanoparticle, and the length is more than 2 μm. Figure 10(c) is a high magnification image of Fig. 10(b), and the BN nanotube has a bamboo-type structure, as indicated by an arrow. BN nanocoil was also produced, as shown Fig. 10(d), and a Fe nanoparticle is observed as indicated by an arrow. In the case of using magnetic materials as the catalysis metal for BN nanotubes, the magnetic nanoparticles move or rotate with the change of magnetic field, which arises from a coil heater, in the process of reaction. Therefore, it is considered that BN nanocoils were produced. High WR of Fe_4N would be suitable for synthesis of BN nanocoils because the frequency of moving is high with increasing of the amount of magnetic nanoparticles. Bamboo-type BN nanotubes were also observed, as shown in Fig. 10(e) and 10(f). Nanoparticles were observed at the root of the nanotubes, which would be closely related with BN nanotube growth.

Figure 11(a) is a TEM image of BN nanotubes with bamboo-structures. Lengths and widths of BN nanotubes are approximately 5–10 μm and 40–200 nm, respectively. In addition, iron nanoparticles were often observed at the tip of nanotubes, as shown in Fig. 11(b). Enlarged images of a tip and an interface between the Fe nanoparticle and the nanotube are shown in Fig. 11(c) and 11(d), respectively. In Fig. 11(c), amorphous structures (AM) and lattice fringes of Fe_2B {200} are observed near the growth point of BN layers. The amorphous structure would be boron-rich phase formed from reaction with Fe_4N. At the interface between the Fe particle and BN nanotube in Fig. 11(d), lattice fringes of Fe {110} are observed, and the BN {002} layers are inclined from the nanotube axis indicate by z-axis.

A small amount of nanocrystalline Fe_2B compounds were observed at the tip of the BN nanotube (Fig. 12). Chemical formulas that Fe_4N reacts with B, and generates Fe and BN in the experiments can be proposed as follows:

$$Fe_4N + 3B = BN + 2Fe_2B \quad (1)$$

Fe_2B and dissolution of boron were obtained, and BN was produced in the reaction expressed as eq. (1) because Fe_2B is thermodynamically more stable than Fe_4N. Although the

Fe_2B is stable to 1389 °C, the Gibbs-Thompson effect shown that the melting occurs at a significantly lower temperature compared to values in the standard phase diagram. Therefore, fluid-like Fe_2B can be attained more easily. In the next process, the reaction expressed as eq. (2) would take place.

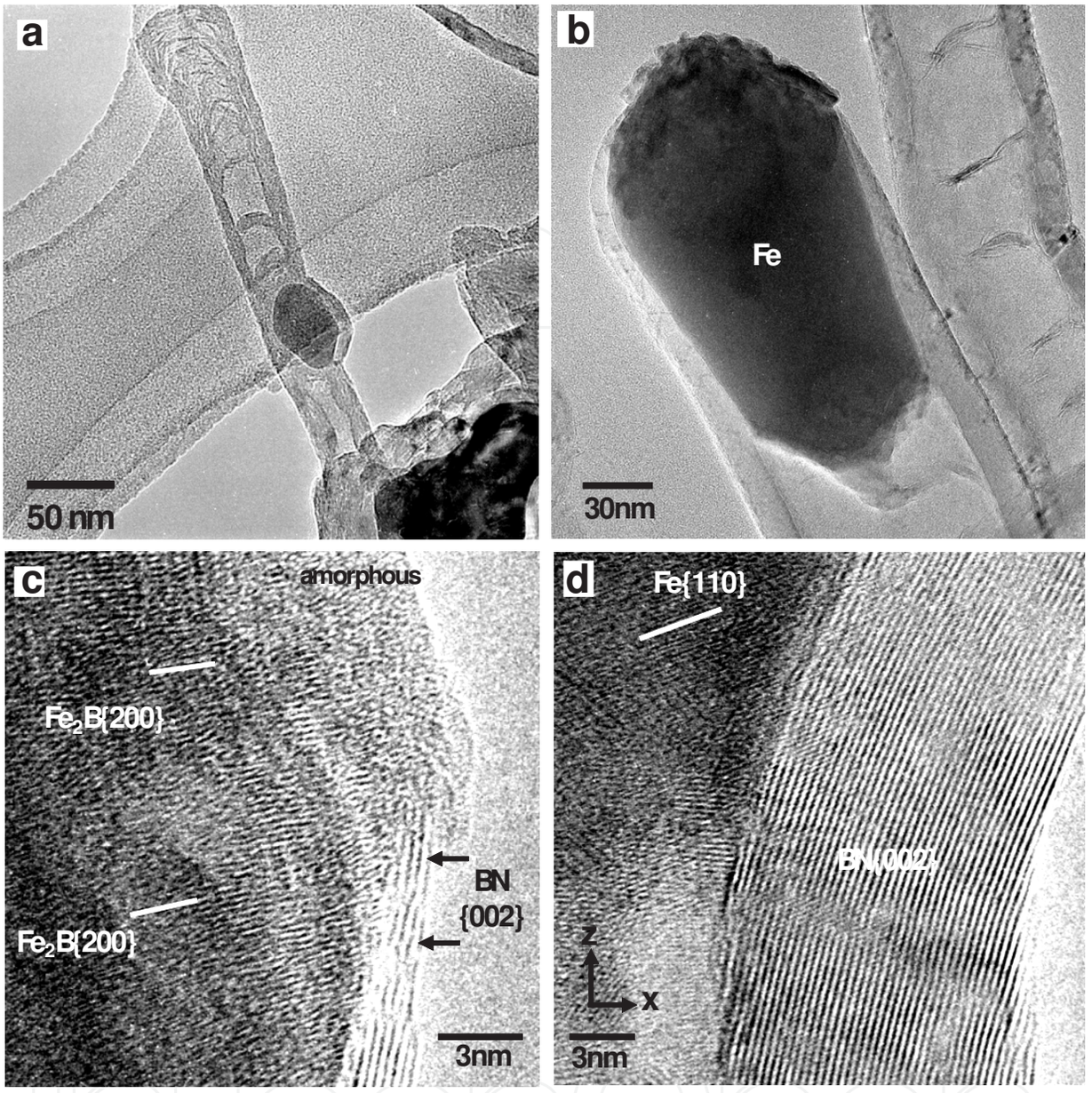

Figure 11. Low magnification images of (a) BN nanotubes with bamboo-structures and (b) iron nanoparticle at a tip of nanotube. Enlarged images of (c) a tip and (d) an interface between the Fe nanoparticle and the nanotube.

$$2Fe_2B + N_2(g) = 2BN + 4Fe \tag{2}$$

Boron in liquid-like Fe_2B started to segregate on the surface of the particle. The boron would react with N_2 gas, and BN was produced. α-Fe in liquid-like Fe_2B is epitaxially grown to the [110] direction, and Fe nanowires were produced in the reaction of eq. (2). In adeition, high WR would be mandatory for the formation of Fe-filled BN nanotubes. As the results of these reactions, the [110] of Fe is parallel to the BN nanotube axis.

http://dx.doi.org/10.5772/51968

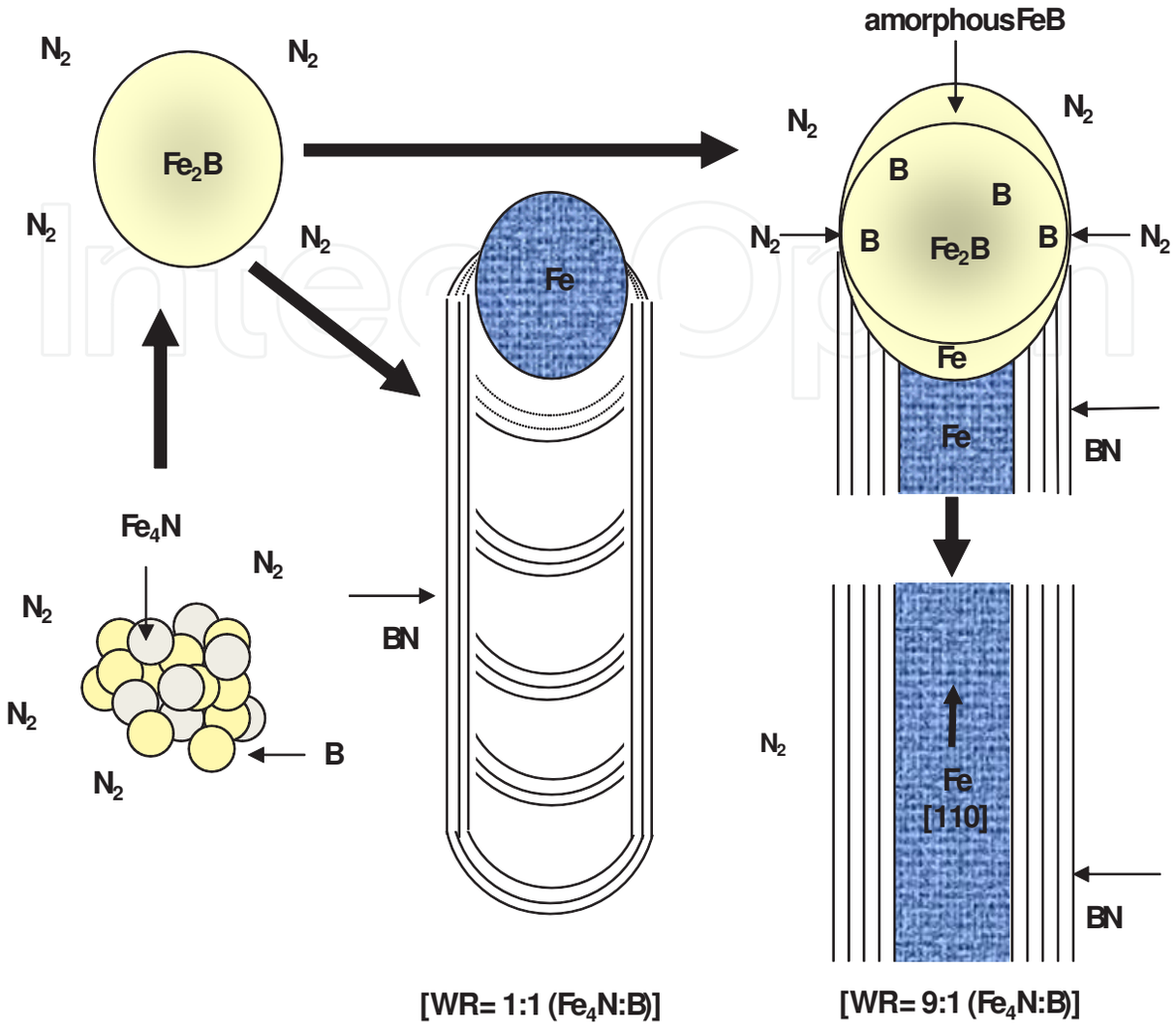

Figure 12. Schematic illustration of the formation mechanism of bamboo-type structure and Fe-filled BN nanotube.

Gibb's energy on each formula is calculated as -89:4 and -23:2 kcal for the formulas (1) and (2) at 1000 °C, respectively. These negative values would stand for correctness of the proposed formulas. It is considered that a formation of Fe-B compounds might plays an important role for growth of the BN nanotubes, and that amorphous boron might change to BN and Fe_2B on the surface of the Fe4N nanoparticles. When magnetic materials are used as catalysis metals for BN nanotube formation, the magnetic nanoparticles would move around by magnetic field of a coil heater during the reaction process. Then, segments of BN {002} layers were produced in the tubes, which results in formation of bamboo structures as shown in Fig. 12. The interval of the BN layer segments might be related to the amount of iron nanoparticles, and further studies are expected on the control of the bamboo structure.

2.3. Purification of BN nanotubes

Selective synthesis and purification methods for BN nanotubes are required to use them as devices, and an efficient method for purification of BN nanomaterials is required. The key steps in purification of BN nanomaterials in the present work would be HCl, HNO_3 and pyridine treatment (Koi et al. 2008).

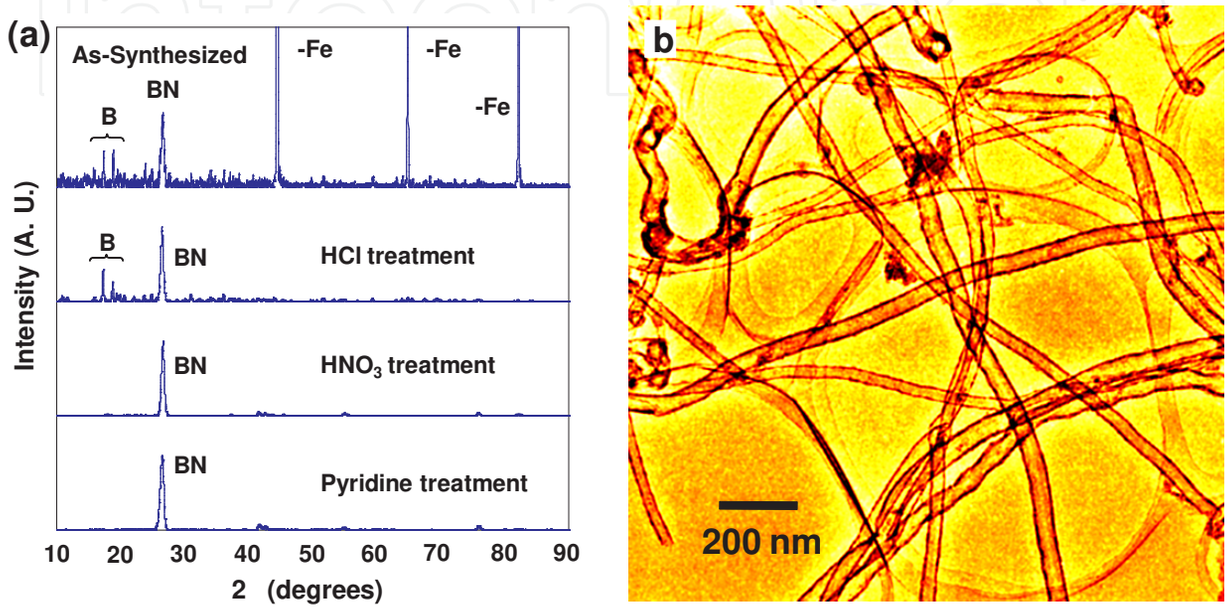

Figure 13. a) X-ray diffraction patterns of samples after synthesis, HCl treatment, HNO_3 treatment, and pyridine treatment. (b) TEM image of samples after pyridine treatment.

As-produced soot synthesized from Fe_4N/B via the above method was purified by the following steps. The as-produced soot were poured in 4 M HCl solution and stirred for 4 h at a room temperature. The green color of the solution provides an indication of the dissolution of Fe ions. After HCl treatment, the samples were poured in 1 M HNO_3 solution and stirred for 30 h at 50 °C. The yellow color of the solution provides an indication of the dissolution of boron. After both acid treatment, the solution was filtered and rinsed with deionized water until the pH of the filtrate became neutral and dried. Then, the samples were poured in pyridine to eliminate bulk BN, and high purity BN nanotubes with a cup-stacked structure were obtained by collecting supernatant.

X-ray diffraction patterns in a purification process are shown in Fig. 13(a). Diffraction peaks of hexagonal BN, boron and α-Fe are observed for the sample at annealed at 1000 °C for 1 h as shown in Fig. 13(a). It is found that Fe was removed after HCl treatment, and boron was removed after HNO_3 treatment. After pyridine treatment, a strong peak of BN was obtained as shown Fig. 13(a). Figures 13(b) show a TEM image of the sample, and there is no obvious change of the structure during the purification process, and BN nanotubes with small sizes were obtained after pyridine treatment. It is believed that bulk

http://dx.doi.org/10.5772/51968

size of BN was eliminated and high purity BN nanotubes were obtained by pyridine treatment. Purification of BN nanotubes were carried out by HCl, HNO_3 and pyridine treatment to remove non-BN nanotubes such as metal catalysts, boron oxides and unreacted boron.

2.4. Nanotube growth from iron-evaporated boron

The purpose is to synthesize BN nanotubes by a normal thermal annealing method. To synthesize BN nanotubes, a Fe thin film was selected and used as a catalyst for nanotube growth in the present work. Boron (B) powders with a particle size of 45 μm (99%, Kojundo Chemical Laboratory) were used as starting materials. B powder was pressed at 100 kg mm^{-2} into pellets with the size of 4 mm height and 15 mm in diameter. Fe with a thickness of *ca.* 10 nm was evaporated on the compact at ~10^{-6} torr, and the Fe would have an island structure. The samples were set on an alumina boat and annealed in a nitrogen atmosphere. The furnace was programmed to heat at 6 °C/min from a room temperature to 1000 °C and hold for 1 h, and then cooled at 3 °C/min to a room temperature. N_2 gas pressure was 0.10 MPa, and its gas flow was 100 sccm.

SEM image of surface of the Fe-evaporated B compact after annealing is shown in Fig. 14(a). Agglomerated BN nanotubes with diameters in the range of 10–20 nm are observed, and they have a network-like structure. Fig. 14(b) is a TEM image of BN nanotubes which were removed from the pellet. Diameters and lengths of BN nanotubes are in the range of 10–20 nm and 100–500 nm, respectively, and the diameters agree well with those of SEM images in Fig. 14(a). One of the typical BN nanotubes is shown in Fig. 14(c), and a nanotube axis is indicated by z. Fig. 14(d) is a Fourier filtered HREM image of center of the same BN nanotube in Fig. 14(c), and hexagonal net planes of BN nanotube are observed clearly in the image of Fig. 14(d). A hexagonal BN ring is shown in Fig. 14(d), and the BN has a zigzag-type structure, as shown in Fig. 14(e).

Growth of carbon nanotubes was explained as a model of vapor-liquid-solid (VLS) mechanism [19]. In this model, hydrocarbon such as methane is resolved in catalyst metal nanoparticles. Supersaturated solid solution of carbon in catalyst metal was precipitated as carbon nanotubes. BN nanotube growth might be explained in a similar model. Schematic illustration of growth mechanism of BN nanotubes was proposed as shown in Fig. 15. Supersaturated solid solution of B in Fe nanoparticles was formed and reacted with N_2 gas. BN nanotubes grow from these sites, and the diameter of nanotubes depends on the particle size. Fe nanoparticles are easy to be separated from BN because Fe begins to react with BN from 1350 °C, and BN nanotubes would grow as shown in Fig. 15. Oriented BN nanotubes might be obtained when Fe nanoparticles are uniformly dispersed on surface of B.

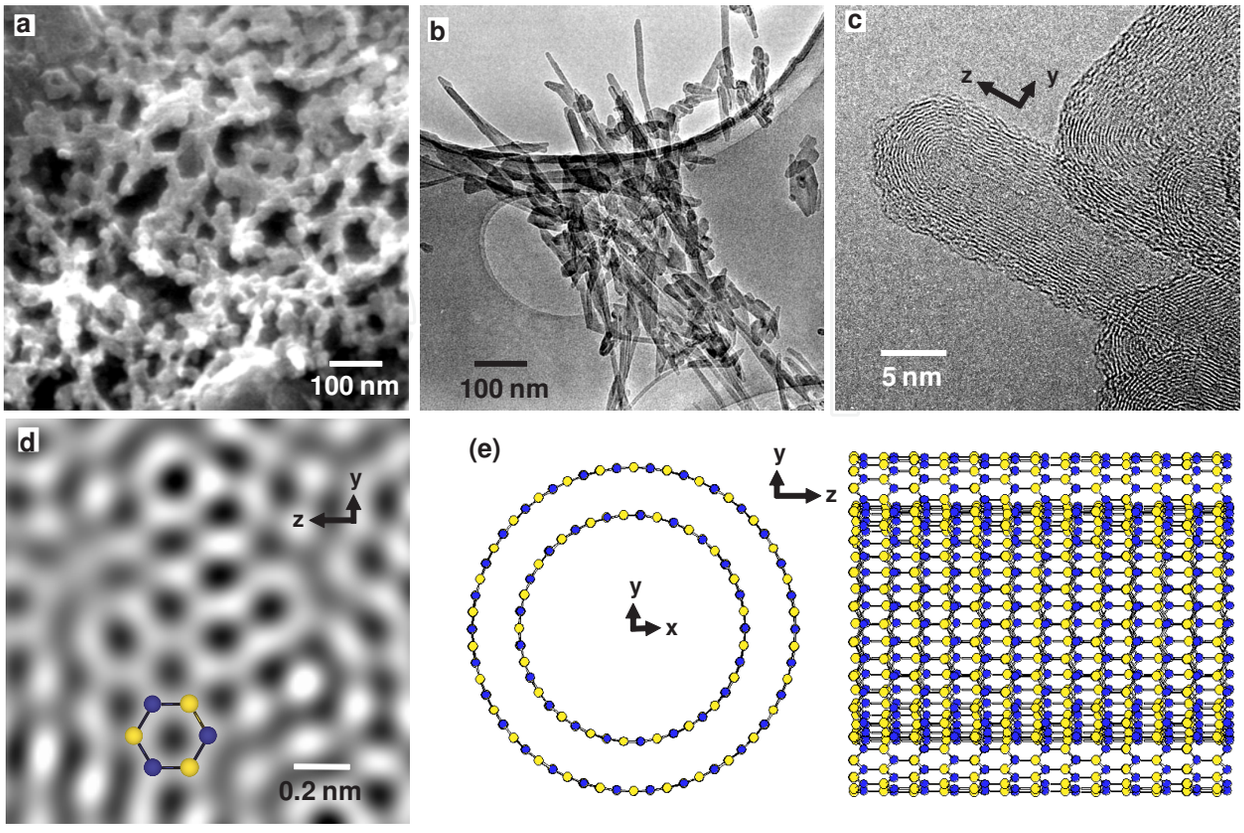

Figure 14. a) SEM and (b) TEM images of BN nanotubes grown from the Fe/B pellet. (c) HREM image of BN nanotube. (d) Enlarged image of the center of BN nanotube in (c). (e) Atomic structure model of zigzag-type BN nanotube.

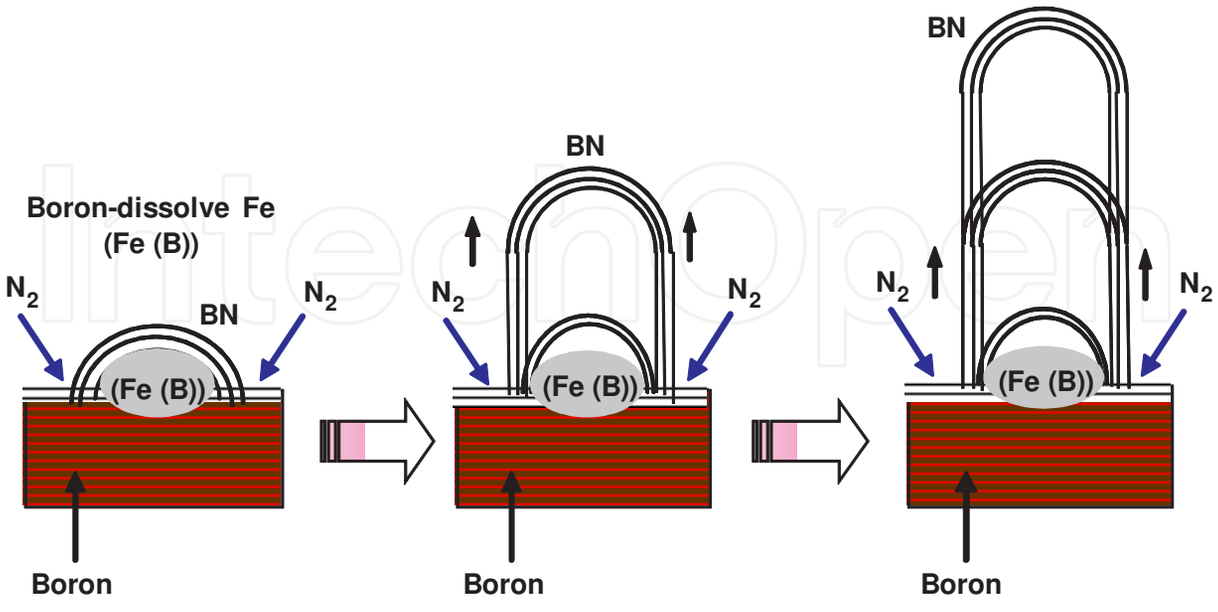

Figure 15. Schematic illustration of the growth mechanism of BN nanotubes.

http://dx.doi.org/10.5772/51968

3. Atomic structures of BN nanotubes

3.1. Chiralities of BN nanotubes

A low magnification TEM image of BN nanotubes produced from YB_6/Ni powder is shown in Fig. 16(a) (Oku & Narita 2004). The lengths and diameters of BN nanotubes are ~5 μm and 3–50 nm, respectively. Fig. 16(b) is an EELS spectrum of BN nanomaterials including BN nanotubes. Two distinct absorption features are observed at 188 and 401 eV, which correspond to boron K-edge and nitrogen K-edge onsets, respectively. The fine structure of boron in the EELS spectrum shows the hexagonal bonding between boron and nitrogen, which is indicated by presence of a sharp π* peak and the shape of the σ* peak. The EELS spectrum also shows the weak σ* peaks of B and N, which indicate the spherical structure of BN nanomaterials.

A HREM image of a $B_{36}N_{36}$ cluster inside a BN nanotube is shown in Fig. 16(c). The BN nanotube has a multiwalled structure, and a diameter of the most inner tube is 1.75 nm. An atomic structure model of the center of Fig. 16(c) is shown in Fig. 16(d). Diameter and chirality of the BN nanotube are 1.747 nm and (22, 0), respectively. This kind of peapod-type self-organized structure would be useful for the nanoscale devices. Another HREM image of BN nanotubes with a bundled structure is shown in Fig. 16(e), and an atomic structure model observed from three different directions is shown in Fig. 16(f). There are some spaces among the BN nanotubes, and the space would be useful for gas storage such as hydrogen.

Figure 17(a) is a HREM image of a quadruple-walled BN nanotube. In the present work, all HREM images were taken close to the Scherzer defocus (Δf_S = −41.2 nm), which is an optimum defocus value of electron microscope, in order to investigate the atomic structures in detail. HREM observations and electron diffraction analysis on BN nanotubes have been reported, and direct observations of nanotube chirality were tried in the present work. An enlarged HREM image is shown in Fig. 17(b), which indicates lattice fringes in the BN nanotubes.

A filtered Fourier transform of Fig. 17(b) showed that this nanotube had a zigzag-type structure as shown in Fig. 17(c) (Oku 2011). A HREM image with clear contrast processed after Fourier noise filtering is shown in Fig. 8d. The intervals of the bright and dark dots are 0.14 nm, which corresponds to the structure of h-BN rings, as shown in Fig. 17(e). Layer intervals of each tube are 0.35 nm, as shown in Fig. 17(f). Diameters of each nanotube are 2.8, 3.5, 4.2, and 4.9 nm from the inside to outside.

Another HREM image of BN nanotube produced from YB_6 powder is shown in Fig. 18(a). Width of the multiwalled BN nanotube is 8.5 nm. The BN nanotube consists of nine layers and has asymmetry layer arrangements. Layer distances are in the range of 0.34–0.51 nm, which is larger than that of {002} of ordinary h-BN (0.34 nm). Diameters of the first and second internal nanotubes are 1.7 nm and 2.6 nm, respectively. Hexagonal net planes of BN nanotube are observed in an enlarged image of Fig. 18(b). Figure 18(c) is a filtered Fourier transform of Fig. 18(b), which indicates 002 and 100 reflections of BN structure. Inverse Fourier transform of Fig. 18(c) is shown in Fig. 18(d), which indicates the lattice fringes of hexagonal networks clearly. A h-BN ring is shown in Fig. 18(d), and the BN has an armchair-type structure.

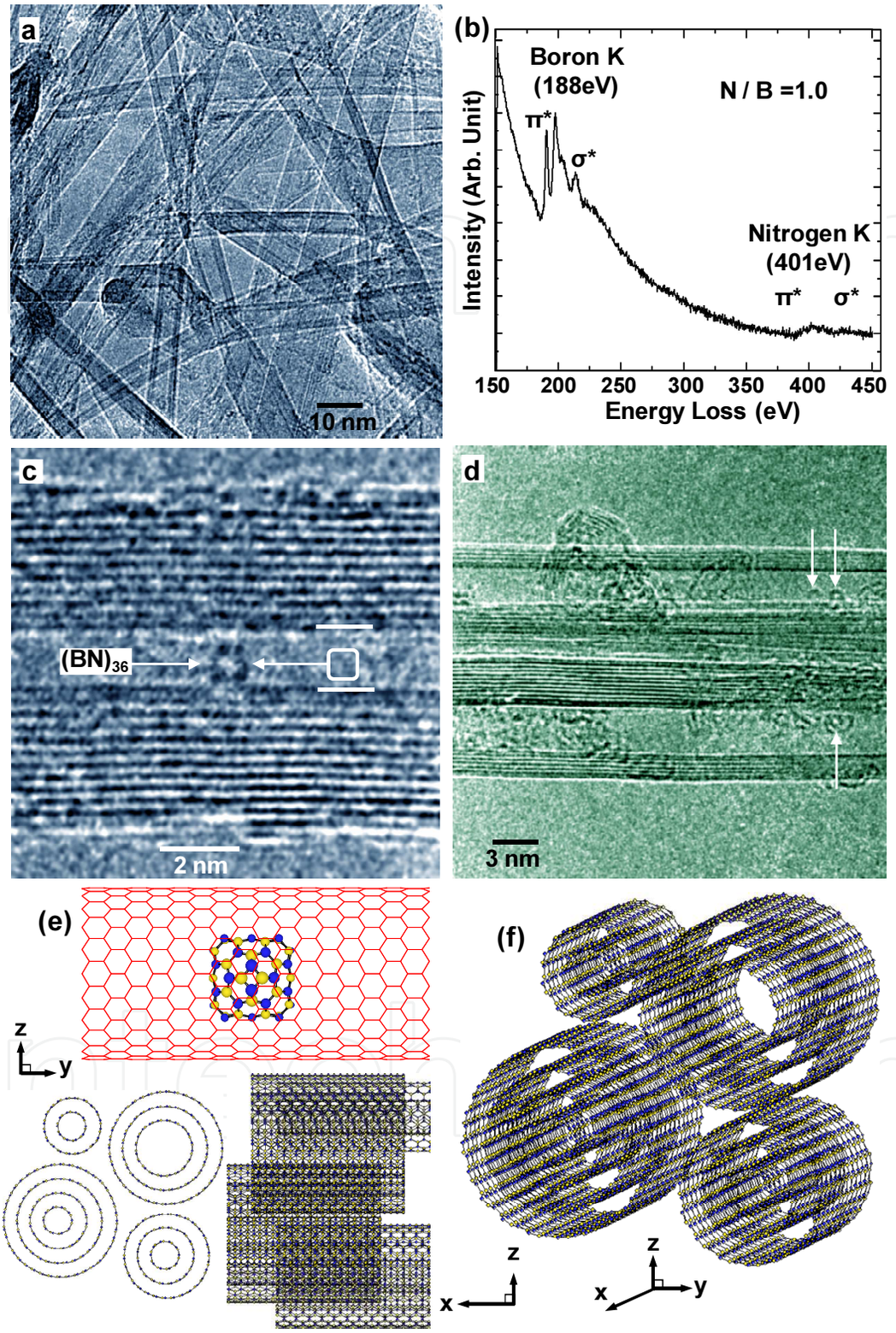

Figure 16. a) TEM image and (b) EELS spectrum of BN nanotubes. (c) HREM image of $B_{36}N_{36}$ cluster in BN nanotube. (d) HREM image of bundled BN nanotubes. BN clusters are indicated by arrows. (e) Structure model of the center of (c). (f) Atomic structure model from three different directions for bundled BN nanotubes

http://dx.doi.org/10.5772/51968

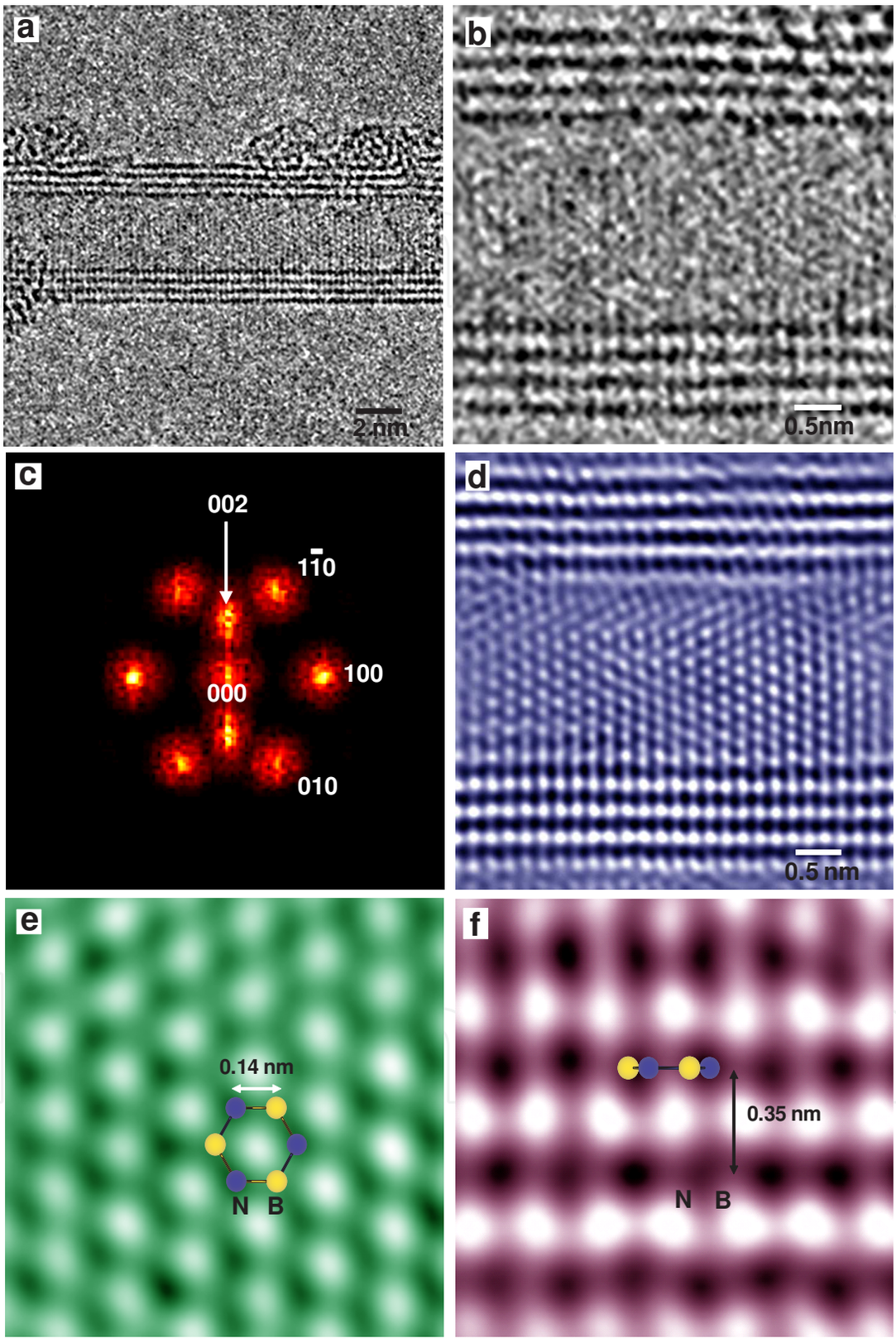

Figure 17. a) HREM image of zigzag-type BN nanotube. (b) Enlarged HREM image of (a). (c) Filtered Fourier transform of (b). (d) Inverse Fourier transform of (c). Enlarged images of center (e) and edge (f) of the BN nanotube in (d).

Atomic structure models were proposed from observed diameters of BN nanotubes, which were based on layer intervals of 0.34–0.35 nm. The chirality of (n, m) is derived from the equation

$$d_t = \frac{\sqrt{3}a_{B\text{-}N}\sqrt{n^2 + nm + m^2}}{\pi} \tag{3}$$

The d_t means a diameter of BN nanotube with nm scale, and the a B-N corresponds to the nearest distance of boron and nitrogen atoms. For the BN nanotubes, the value of a B-N is 0.144 nm. When a BN nanotube has a zigzag structure, the value of m is zero.

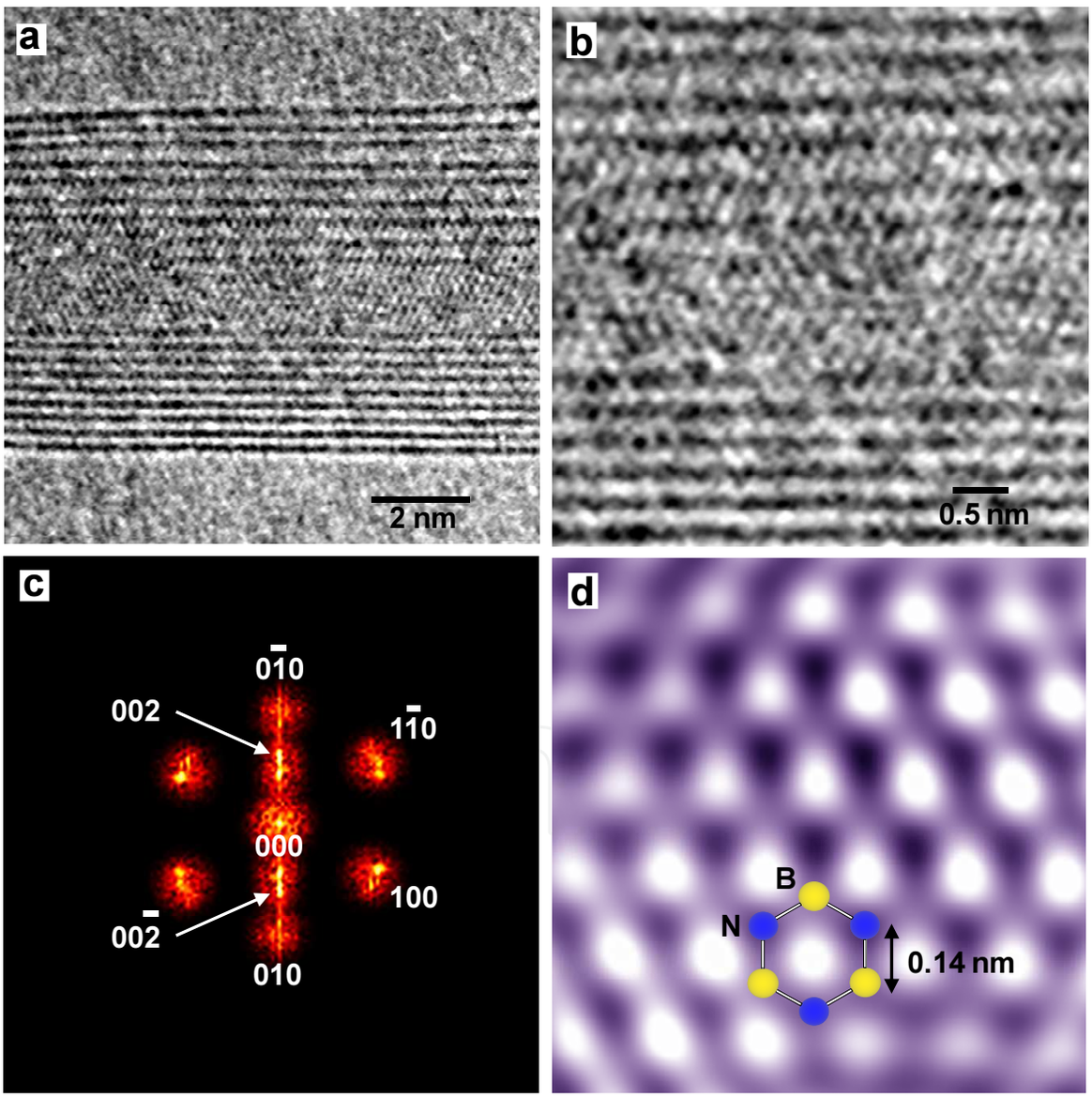

Figure 18. a) HREM image of armchair-type BN nanotube. (b) Enlarged HREM image of (a). (c) Filtered Fourier transform of (b). (d) Inverse Fourier transform of (c).

http://dx.doi.org/10.5772/51968

Figure 19(a) shows a proposed structure model of the quadruple-walled BN nanotube. Chiralities of each zigzag BN nanotube are (35, 0), (44, 0), (53, 0), and (62, 0) from the inside to outside. These chiralities were derived from (3). The arrangement of boron and nitrogen atoms was reversed at each layer, as boron atoms exist just above the nitrogen atoms while maintaining the layer intervals of 0.35 nm. Calculated images of the proposed model as a function of defocus values are shown in Fig. 19(b). Contrast of hexagonal rings was clearly imaged at the defocus values in the range of −40 to −50 nm, and these simulated images agree well with the observed HREM image of Fig. 17(d).

A proposed structure model of double-walled BN nanotube corresponding to Fig. 18 is shown in Fig. 19(c). Chiralities of the BN nanotube are (13, 13) and (19, 19) for the first and second layers, respectively. Layer intervals of lattice fringes of {002} planes are accorded with observed ones in Fig. 18(a). Based on the projected structure model, image calculations were carried out for various defocus values, as shown in Fig. 19(d) and a HREM image calculated at −40 nm agrees well with the experimental data of Fig. 18(d).

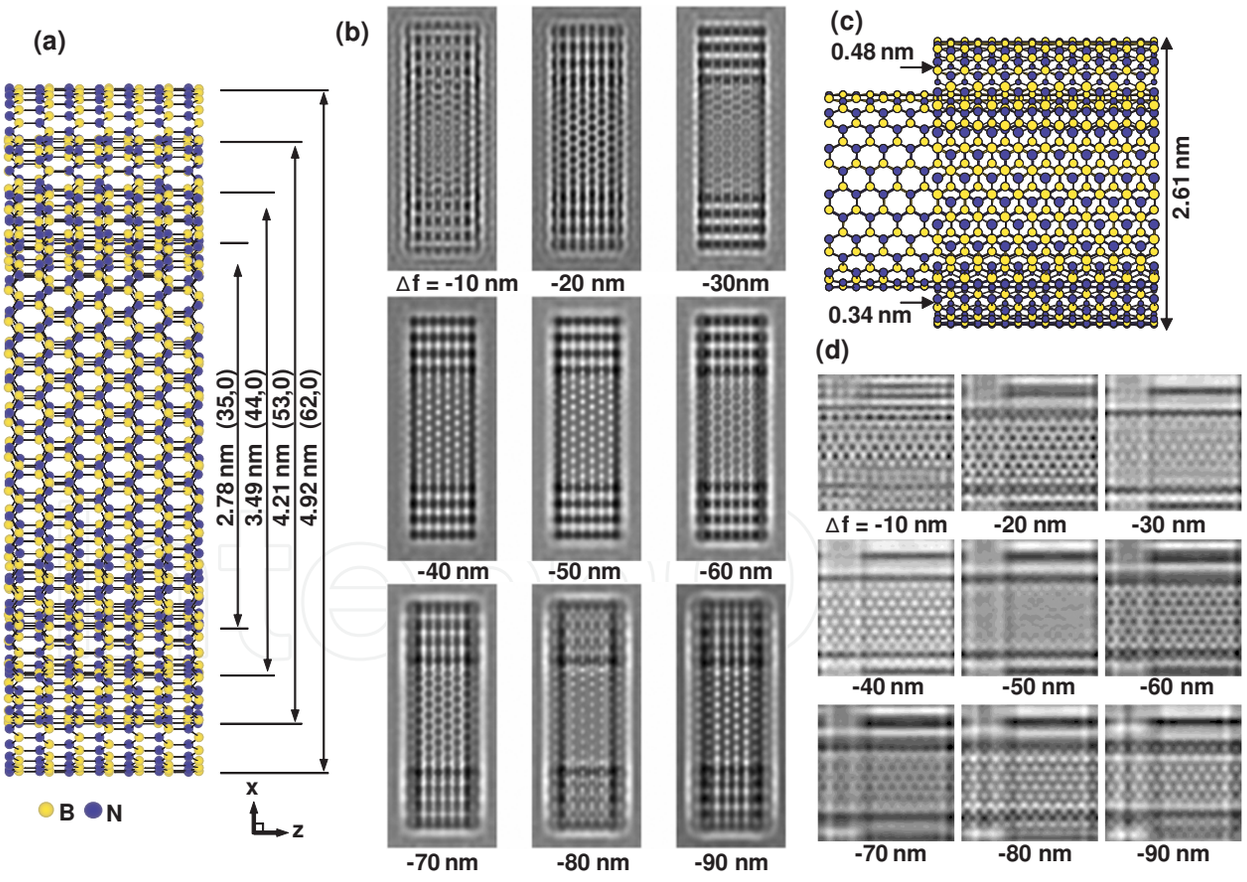

Figure 19. a) Proposed structure model of quadruple-walled BN nanotube. Chiralities of zigzag BN nanotubes are (35, 0), (44, 0), (53, 0), and (62, 0) from inside to outside. (b) Calculated images of the proposed model (a) as a function of defocus values. (c) Proposed structure model of doublewalled BN nanotube. Chiral vectors of nanotube are (13, 13) and (19, 19) for the first and second layers, respectively. (d) Calculated images of the proposed model (c).

3.2. BN nanotubes with cup-stacked structures

Figure 20(a) shows TEM image of BN nanotubes with a cup-stacked structure after purification process (Oku et al. 2007). Diameters and lengths of the BN nanotubes are in the range of 40-100 nm and 5-10 μm, respectively. Fe nanoparticles and bulk BN was eliminated during the process. An enlarged image of one of the BN nanotubes is shown in Fig. 20(b), which shows a cup-stacked structure as indicated by lines of BN {002}. Figure 20(c) is an electron diffraction pattern of Fig. 20(b). 002 reflections of BN are splitting in Fig. 20(c), which indicates that the BN nanotube has a cup-stacked structure and the cone angle between the BN layers at both nanotube walls is ~20°. Most of BN nanotubes (~90%) have this cup-stacked structure with cone angle of ~20°, and normal structures with a cone angle of 0° were sometimes observed (~10%). An optical absorption spectrum of BN nanotubes is shown in Fig. 20(d). In Fig. 20(d), a strong peak is observed at 4.8 eV, which would correspond to the energy gap of BN nanotubes. A broad, weak peak is also observed around 3.4 eV, which is considered to be impurity level (oxygen or hydrogen) of the BN layers. Comparable data (4.5-5.8 eV) were reported for other optical measurements (Lauret et al. 2005).

A HREM image of edge of the nanotube side wall in Fig. 20(b) is shown in Fig. 21(a), and a cup-stacked structure was observed. Edge structures are observed as indicated by arrows, and the BN {002} planes are inclined compared to nanotube axis (z-axis). Figure 21(b) is a processed HREM image after Fourier filtering of nanotube center of Fig. 21(b), and hexagonal arrangements of white dots are observed, which would correspond to BN six-membered rings. From these observations, a structure model for BN cup-structure was proposed, which consists only of h-BN rings, as shown in Fig. 21(c) and (d).

Based on the structure model of a four-layered cup-stacked $B_{2240}N_{2240}$ nanotube, an image calculation was carried out as shown in Fig. 21(e). Enlarged calculated HREM images of the edge and the center of the BN nanotube in Fig. 21(e) are shown in Fig. 21(f), 21(g), respectively. These calculated images agree with the experimental data of Fig. 21(a), 21(b), respectively.

As shown in Fig. 20(c), BN layers are often inclined compared to nanotube axis, which are called cup-stacked nanotubes. A HREM image and Fourier filtered image of nanotube wall of bamboo-type BN nanotube with cup-stacked structures (WR = 1:1) is shown in Fig. 22(a) and 22(b), respectively. The nanotube axis is indicated by z-axis. BN {002} layers are inclined compared to the nanotube axis, and the cone angle between the BN layers at both nanotube walls is ~36° (Nishiwaki et al. 2005). An enlarged image of nanotube center is shown in Fig. 22(c), and a HREM image with clear contrast was processed after Fourier noise filtering as shown in Fig. 22(d), which shows hexagonal arrangements of white dots.

A structure model for $B_{494}N_{494}$ cup-layer was proposed, which consists only of hexagonal BN rings. A structure model and calculated HREM images of four-fold walled $B_{1976}N_{1976}$ nanotube with a cup-stacked structure are shown in Fig. 22(e) and 22(f), respectively. The calculated images (Fig. 22(f)) at defocus values of 40 and 50 nm have similar contrast of the HREM images in Fig. 22(b) and 22(d).

http://dx.doi.org/10.5772/51968

In order to investigate the stability of the cup-stacked structure, four types of nanotubes are considered, as shown in Fig. 23. Atomic structure models of double-walled BN nanotubes with zigzag-type and armchair-type structures, respectively, are shown in Fig. 23(a) and 23(b). Atomic structure models of four-layered, cup-stacked BN nanotubes with different cone angles are shown in Fig. 23(c) and 23(d). The values of these structures were summarized as in Tables 2 and 3. Total energies of these four-type structures indicates that BN multilayered nanotubes with and without a cup-stacked structure would be stabilized by stacking h-BN networks.

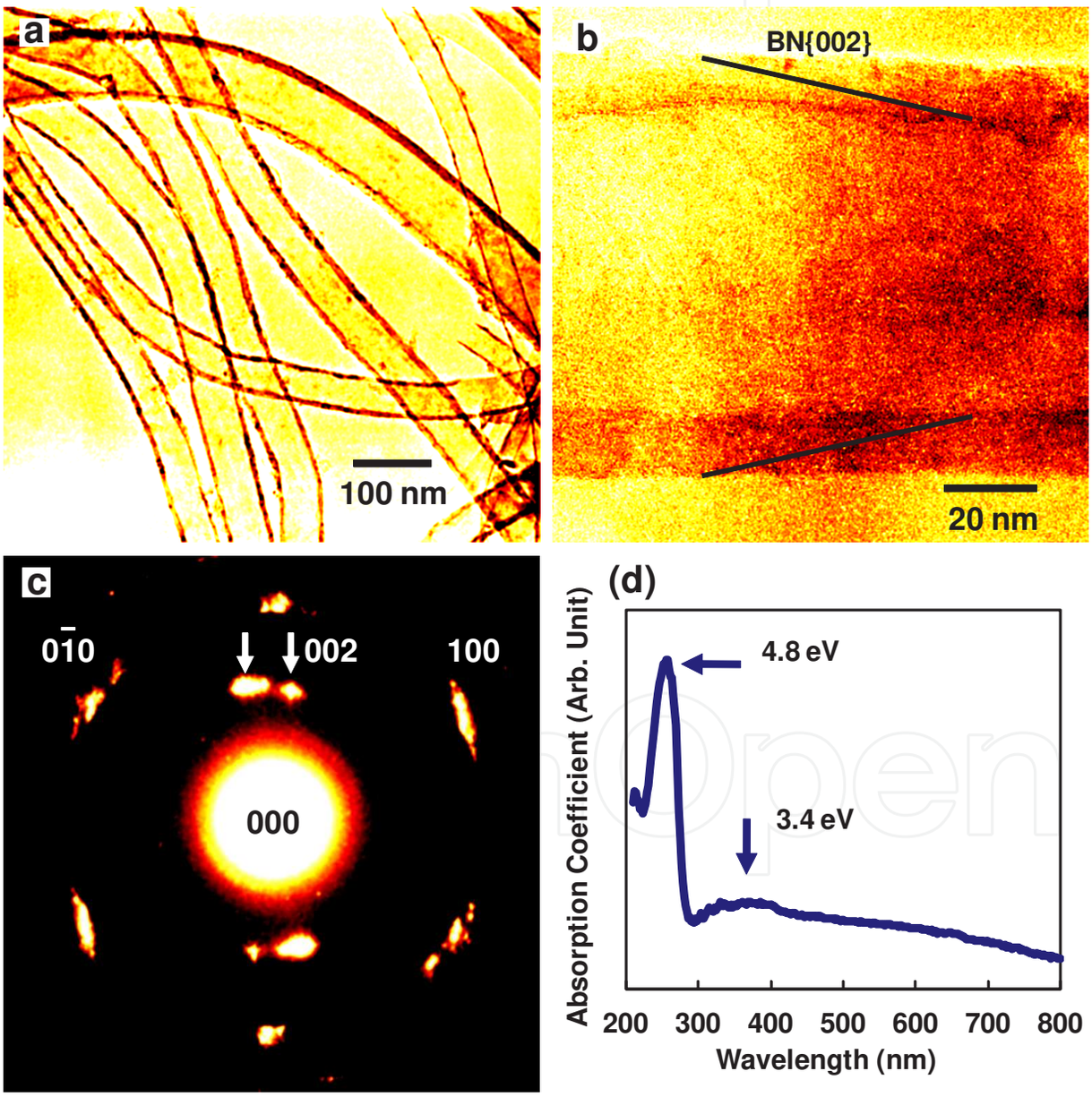

Figure 20. a) TEM image of BN nanotubes after purification. (b) Enlarged image of BN nanotube with cup-stacked structure. (c) Electron diffraction pattern of (b). (d) Optical absorption spectrum of BN nanotubes.

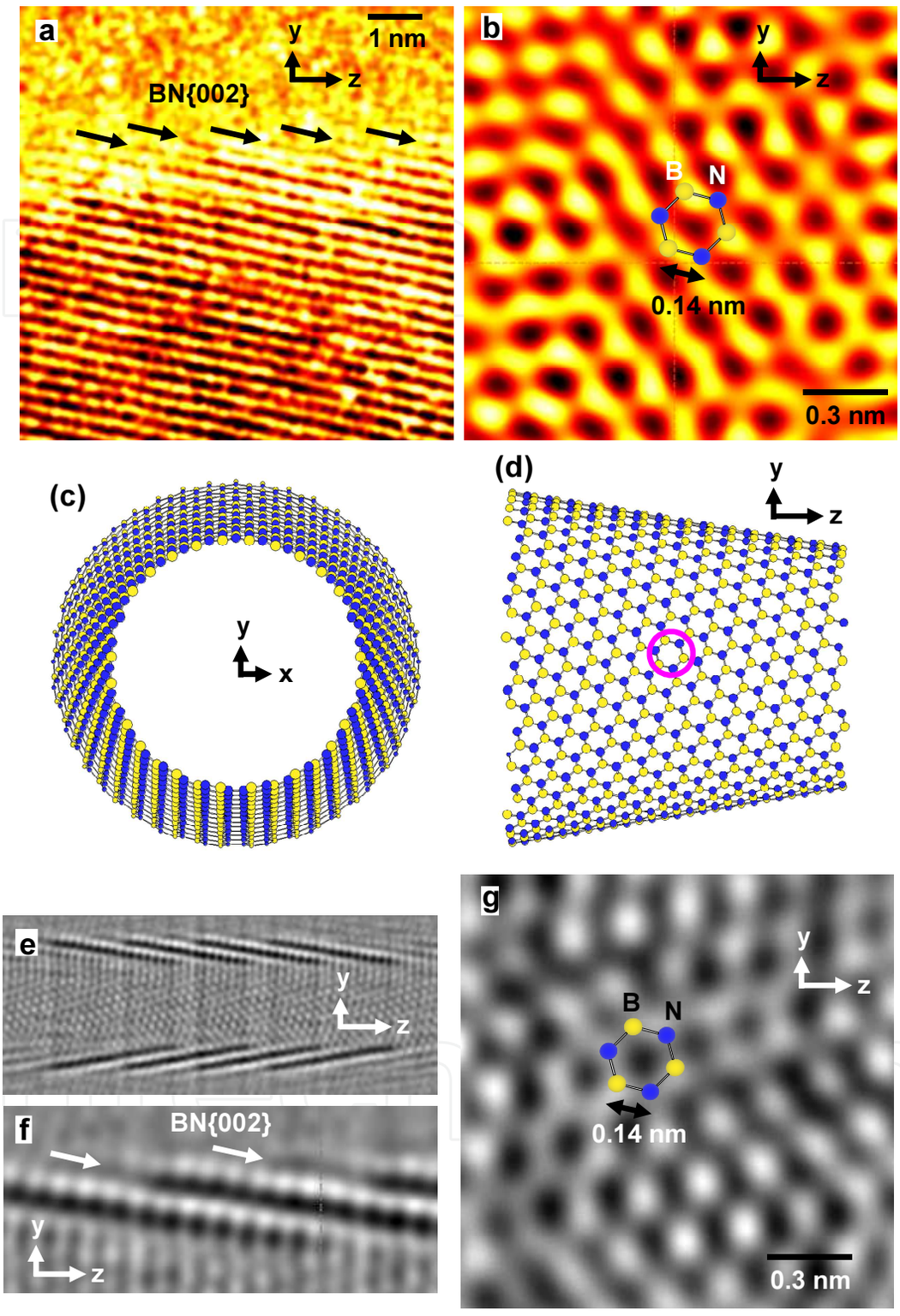

Figure 21. a) HREM image of edge of the BN nanotube wall in Fig. 20(b). (b) Processed HREM image after Fourier filtering of the nanotube center of Fig. 20(b). Proposed model of the BN cup structure projected along (c) the z-axis (nanotube axis) and (d) the x-axis. (e) Calculated HREM image of four-layered, cup-stacked BN nanotube at defocus values of –40 nm. Enlarged image of (f) edge and (g) center of BN nanotube in (e).

http://dx.doi.org/10.5772/51968

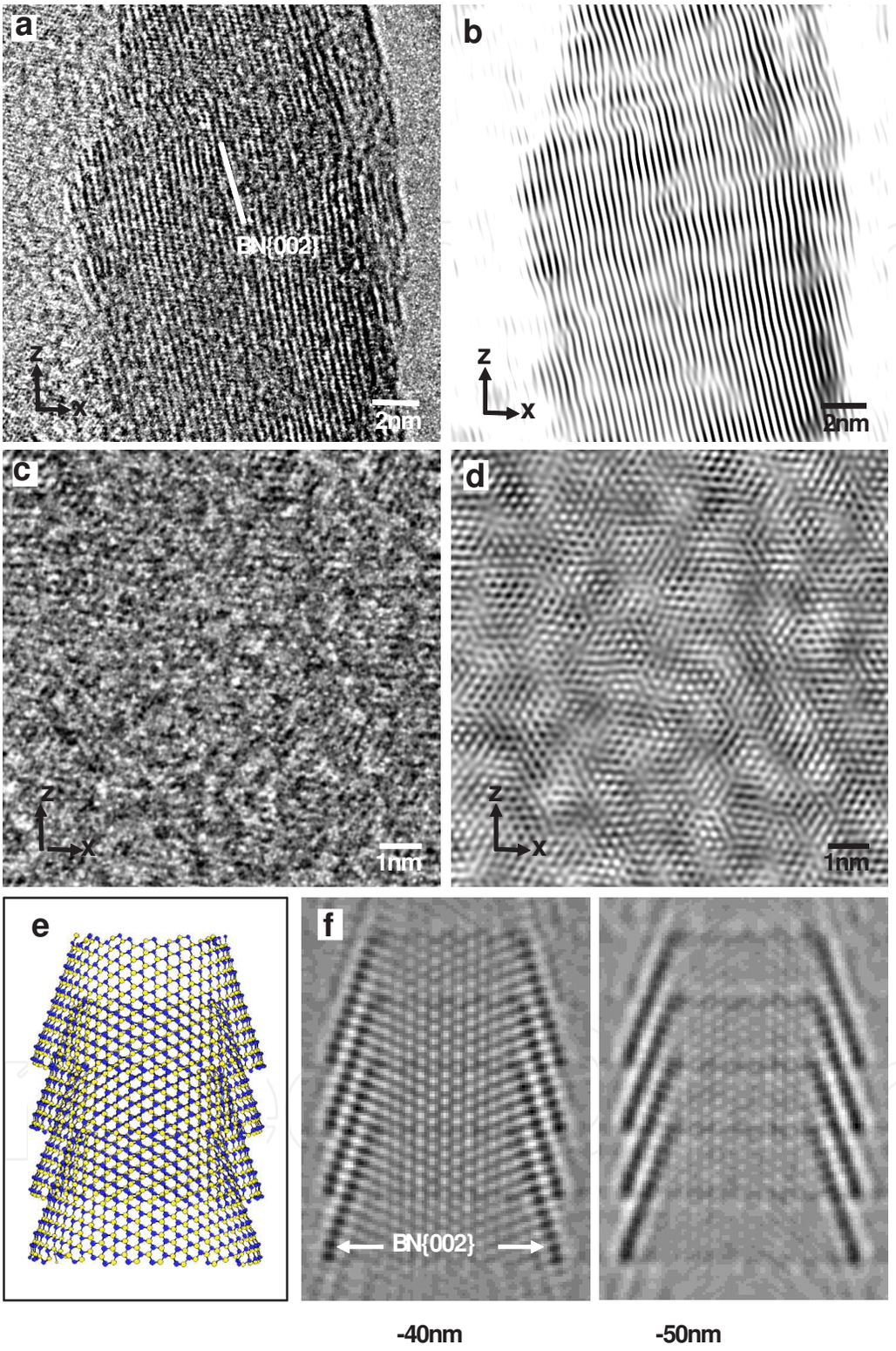

Figure 22. a) HREM image of nanotube wall of bamboo-type BN nanotube with cup-stacked structures. (b) Processed image after Fourier filtering of (a). (c) HREM image of nanotube center. (d) Processed image after Fourier filtering of (c). (e) Processed image after Fourier filtering of (c). (e) Structure model of four-fold walled $B1_{976}N_{1976}$ nanotube with a cup-stacked structure. (f) Calculated HREM images as a function of defocus values.

	$B_{273}N_{273}$	$B_{390}N_{390}$	$B_{273}N_{273}$ @$B_{390}N_{390}$	$B_{264}N_{264}$	$B_{384}N_{384}$	$B_{264}N_{264}$ @$B_{384}N_{384}$
Structure type	Zigzag	Zigzag	Zigzag	Armchair	Armchair	Armchair
Outer diameter (nm)		2.3	2.3		2.2	2.2
Inner diameter (nm)	1.6		1.6	1.5		1.5
Number of layers	1	1	2	1	1	2
Total energy (kcal/mol)	459.2	701.5	556.0	466.6	693.2	779.3
Total energy (kcal/mol·atom)	0.841	0.899	0.419	0.883	0.902	0.601

Table 2. Calculated values for various BN nanotubes

	$B_{560}N_{560}$	$B_{1120}N_{1120}$	$B_{2240}N_{2240}$	$B_{494}N_{494}$	$B_{988}N_{988}$	$B_{1976}N_{1976}$
Corn angle (°)	20	20	20	36	36	36
Outer diameter (nm)	3.4	3.4	3.4	4.2	4.2	4.2
Inner diameter (nm)	2.4	2.4	2.4	2.4	2.4	2.4
Number of layers	1	2	4	1	2	4
Total energy (kcal/mol)	31.456	-287.924	-936.415	895.1	1269	2062
Total energy (kcal/mol·atom)	0.028	-0.129	-0.209	0.906	0.642	0.522

Table 3. Calculated values for various BN nanotubes with a cup-stacked structure.

Distance between BN layers of nanotubes with a cup-stacked structure in a HREM image was found to be ~0.35 nm, and the basic structure model was constructed based on this observation. Geometry optimizations at molecular mechanics level result in the interlayer distances of ~0.38 nm. Comparing the empirical total energies of all the considered structures, a cup-stacked structure ($B_{2240}N_{2240}$) with cone angle of 20° was found to be the lowest in energy, which indicates the high stability of this structure.

The BN nanotubes with cup-stacked structures in the present work would also be one of the candidates for atomic and gas storage, as well as carbon nanotubes. Cone angles of BN cup-stacks were measured to be ~36°, which agreed well with that of the model in Fig. 22(e) (38°). Cone angles of carbon nanotubes with a cup-stacked structure were reported to be in the range of 45–80° (Endo et al. 2003). The cause of the different cone angles of the present cup-stacked BN nanotubes would be due to the different stacking of BN layers along c-axis (B-N-B-N...) from carbon layers. The cone angles might also depend on the shape of catalysis particles, as shown in Fig. 11(b).

http://dx.doi.org/10.5772/51968

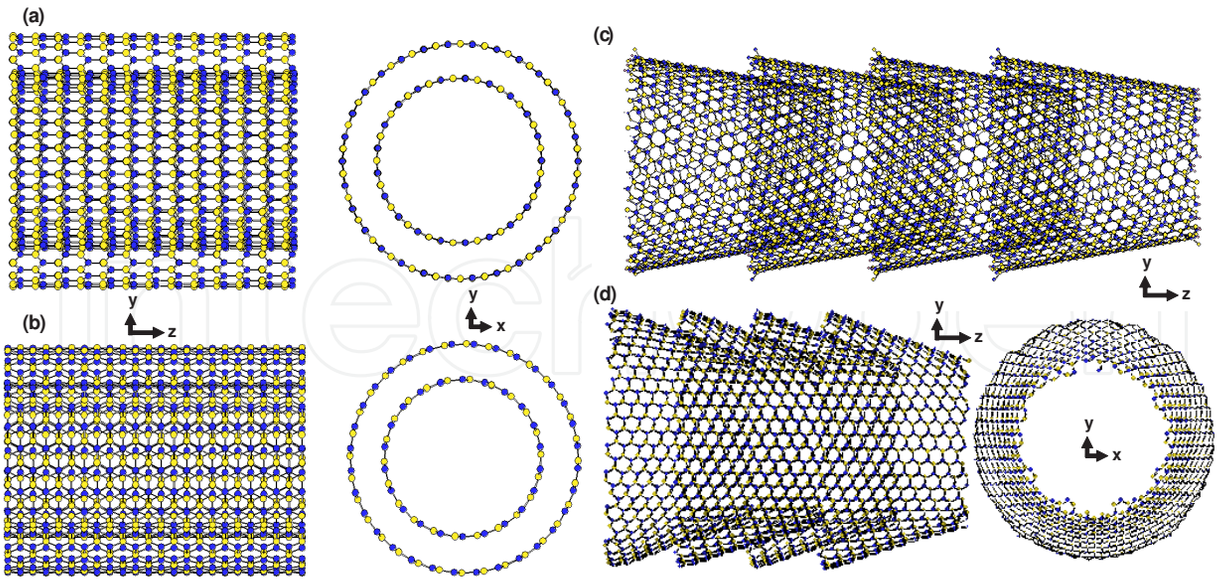

Figure 23. Atomic structure models of double-walled BN nanotubes with (a) zigzag-type and (b) armchair-type structures. Atomic structure models of four-layered, cup-stacked BN nanotubes with cone angles of (c) 20° and (d) 36°

3.3. STM observation of BN nanotube

Although the network structure of carbon nanotubes has already been observed by scanning tunneling microscopy (STM) (Wilder et al. 1998), only few works on the STM observation of the hexagonal plane of BN nanotubes have been reported because of the insulating behavior. The STM image of BN nanotubes on highly oriented, pyrolytic graphite (HOPG) is shown in Fig. 24(a) (Oku et al. 2008). Three BN nanotubes are observed in the image, and the smallest one is selected for enlarged observation and electronic measurements. The nanotube axis is indicated as the z -axis. An enlarged image of the surface of the BN nanotube is shown in Fig. 24(b). The surface of the BN nanotubes is indicated by arrows. A lattice image of the BN nanotubes is observed, and an enlarged STM image of the BN nanotubes is shown in Fig. 24(c). Hexagonal arrangements of dark dots are observed, which correspond to the size of the sixmembered rings of BN. Current-voltage (I-V) measurements were also carried out for the BN nanotubes, as shown in Fig. 24(d). The I–V curve indicates an onset voltage at 5.0 V, which agreed with optical measurement of Fig. 20(d), and is almost comparable to the energy gap of BN nanomaterials. Comparable data were also reported for other STM measurements (Ishigami et al. 2005, Wang et al. 2005).

4. Metal nanowires encapsulated in BN nanotubes

Several studies have been reported on metal-filled BN nanomaterials. Nanowires constructed from magnetic materials, especially Fe, Co and some Fe-based alloys are of interest, because they are likely to be used in nanoelectronics devices, magnetic recording media and

biological sensors. However, the oxidation- and corrosionresistances of surface are weak point of the metallic nanowires. BN nanocables are of potential use for nanoscale electronic devices and nanostructured ceramic materials because of providing good stability at high temperatures with high electronic insulation in air. Therefore, metal-filled BN nanomaterials would have significant advantages for technological application. Although it is reported that Fe-filled BN nanotube could be achieved (Golberg et al. 2003), they still have some problems such as little production and low yield because it is difficult to exist in directly fabricating BN nanocable with metal cores to the poor wetting property of BN to metal.

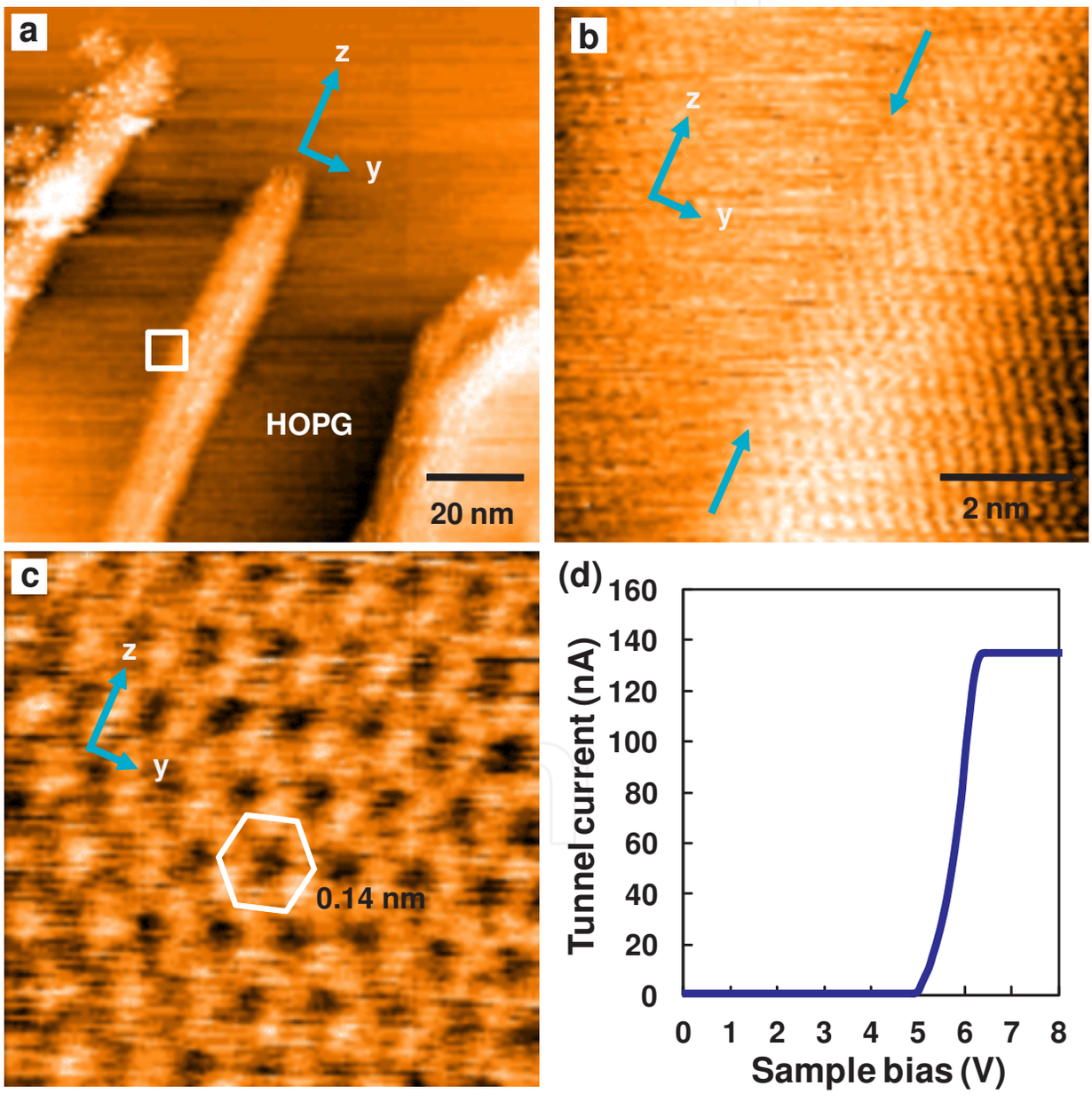

Figure 24. a) STM image of BN nanotubes on HOPG. (b) Enlarged image of the surface of the BN nanotube indicated by a square in (a). (c) Enlarged STM image of the BN nanotube. (d) I - V characteristic of the single BN nanotube.

http://dx.doi.org/10.5772/51968

The purpose of the present work is to synthesis metal-filled BN nanotube and various BN nanomaterials and to investigate the morphology of Fe-filled BN nanotube by HREM, high-angle annular dark-field scanning transmission electron microscopy (HAADF-STEM), electron diffraction and energy dispersive X-ray spectroscopy (EDX). It is possible to use HAADF-STEM to detect single heavy atoms on alight support. Scattering is caused by the nucleus and follows roughly a Z^2 dependence. Fe-filled BN nanotubes could be observed by performing centrifugation. It is considered that centrifugation is effective in collecting Fe-filled BN nanotube because density of Fe is higher than that of BN nanomaterials. Formation mechanism of Fe-filled BN nanotube was proposed based on these results.

Fe_4N (99%, Kojundo Chemical Laboratory (KCL) Co. Ltd., Saitama, Japan) and boron (B) powders (99%, KCL) were used as raw materials. Their particle sizes were about 50 and 45 mm, respectively. After the Fe4N and B (weight ratio WR = 1:1) were mixed by a triturator, the samples were set on an alumina boat and annealed in the furnace. The furnace was programmed to heat at 6 °C/min from ambient to 1000 °C and hold for 1–5 h and then cooled at 3 °C /min to ambient temperature. Nitrogen pressure was 0.10 MPa, and its gas flow was 100 sccm. As-produced soot synthesized via the above method was centrifuged at 8000 rpm for 2 min, and supernatant liquid is removed. The remaining sediments were collected and observed.

Figure 25(a) and 25(b) are TEM and HAADF-STEM images of Fe-filled BN nanotubes (WR = 9:1), which were remaining sediment after centrifugation. The contrast in the TEM image is weak and direct observation of Fe-filled BN nanotubes is difficult. The same area imaged by HAADFSTEM shows excellent contrast and the morphology of Fe-filled BN nanotubes can be observed in detail. A great number of Fe-filled BN nanotubes were observed by HAADF-STEM. High WR of Fe_4N would be necessary for synthesis of Fe nanowires. TEM image of one of Fe-filled BN nanotubes is shown in Fig. 25(c). Figure 25(d) is an EDX spectrum of the Fe-filled BN nanotube. In Fig. 25(d), two peaks of boron, nitrogen are observed. This shows the atomic ratio of B:N = 46.5:53.5, which indicates formation of BN. A strong peak of Fe (0.70 keV) is also observed, while a Cu peak arises from the HREM grid. Figure 25(e) is an enlarged image of Fig. 3(c). Fig. 3(f) is an electron diffraction pattern of the Fe-filled BN nanotube. Strong peaks of BN nanotubes correspond to the planes of (002) of BN. Strong peaks are also indexed as metallic Fe with a bcc structure, and the incident beam is parallel to the [111] zone axis of α-Fe.

Figure 26(a) is an enlarged HREM image of Fig. 25(e), and Fig. 25(b) is filtered Fourier transform of Fig. 26(a) (Oku et al. 2007). Figure 26(c) is inverse Fourier transform of Fig. 26(b), and Fig. 26(d) is an enlarged image of Fig. 26(c). Figure 26(d) shows a lattice image of the bcc Fe-filled BN nanotube. The nanotube axis is parallel to the [110] direction of Fe, which indicates the bcc Fe is epitaxially grown to the [110] zone axis. The tubular layers around the nanowire have an average interlayer spacing of 0.34 nm, which corresponds to the (002) spacing of BN. Figure 26(e) is inverse Fourier transform of Fig. 26(b) using 000, Fe ($01\bar{1}$ and $01\bar{1}$) reflections, and Fig. 26(f) is an enlarged image of Fig. 26(e). Several edge-on dislocations are observed as indicated by arrows, which would be due to lattice distortion produced during Fe-filled nanotube growth. This lattice distortion is also observed as expansion in the electron diffraction pattern of Fig. 3(f), as indicated by arrows. These unique structures would be suitable materials for nanoelectronics devices, magnetic recording media and biological sensors with excellent protection against oxidation and wear.

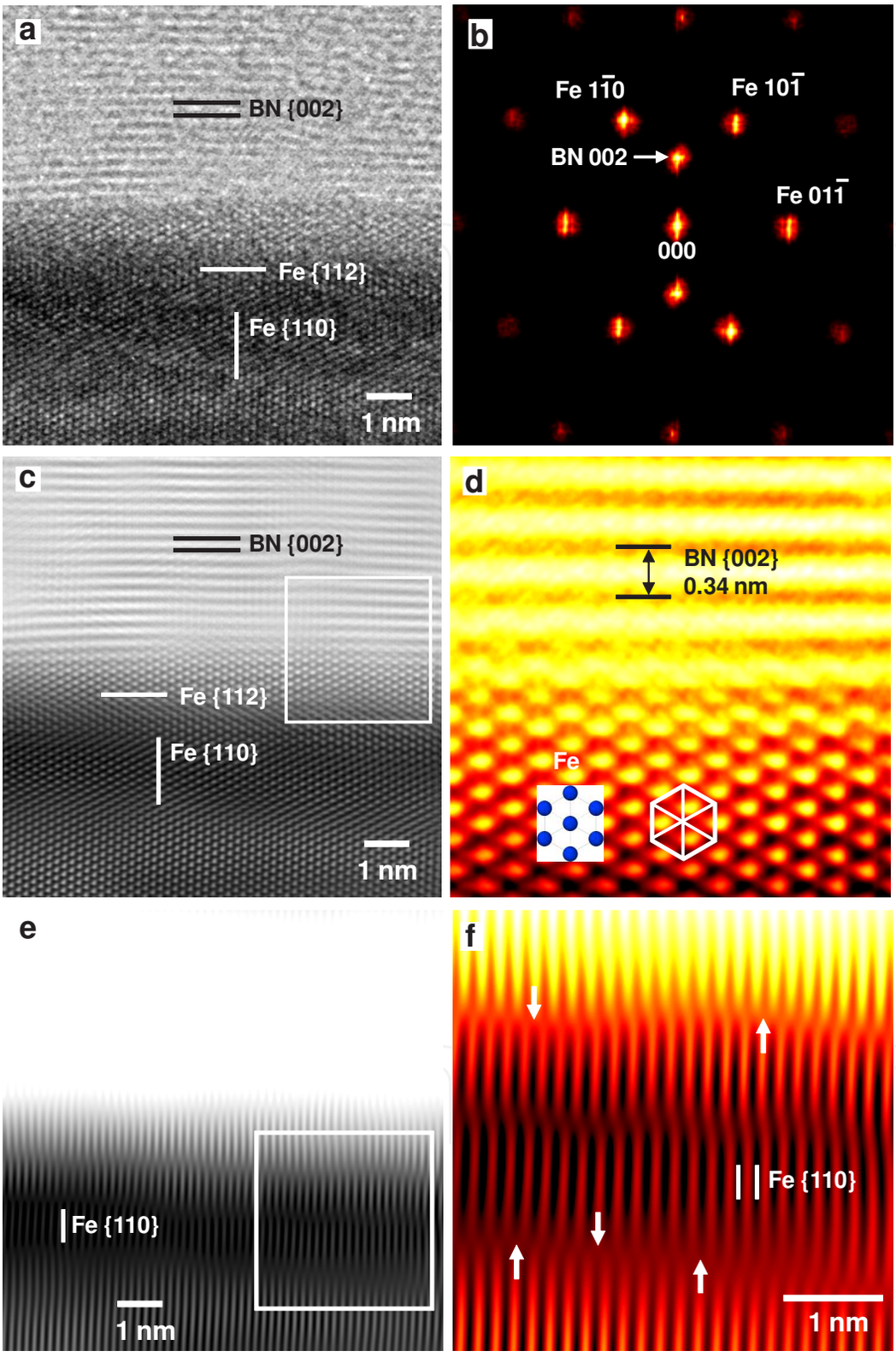

Figure 25. a) TEM and (b) HAADF images of Fe-filled BN nanotubes. (c) TEM image of Fe-filled BN nanotube. (d) EDX spectrum of Fe-filled BN nanotube. (e) Enlarged image of (c). (f) Electron-diffraction pattern obtained from (e).

http://dx.doi.org/10.5772/51968

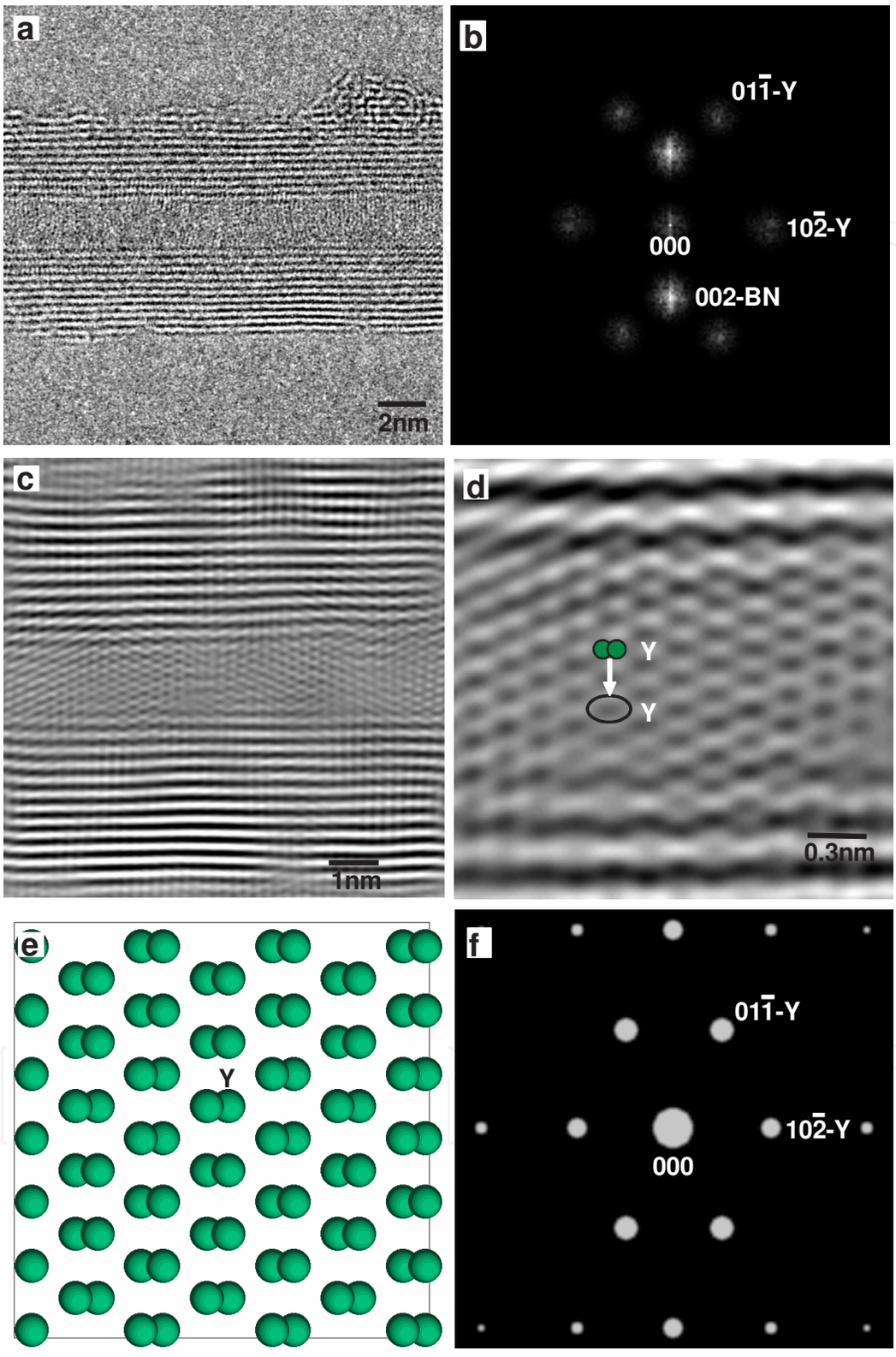

Figure 26. a) HREM image of Fe-filled BN nanotube. (b) Filtered Fourier transform of (a). (c) Inverse Fourier transform of (b). (d) Enlarge image of square in (c). (e) Inverse Fourier transform of (b) using 000, Fe 01$\bar{1}$ and Fe 0$\bar{1}$1 reflections. (f) Enlarged image of square in (e).

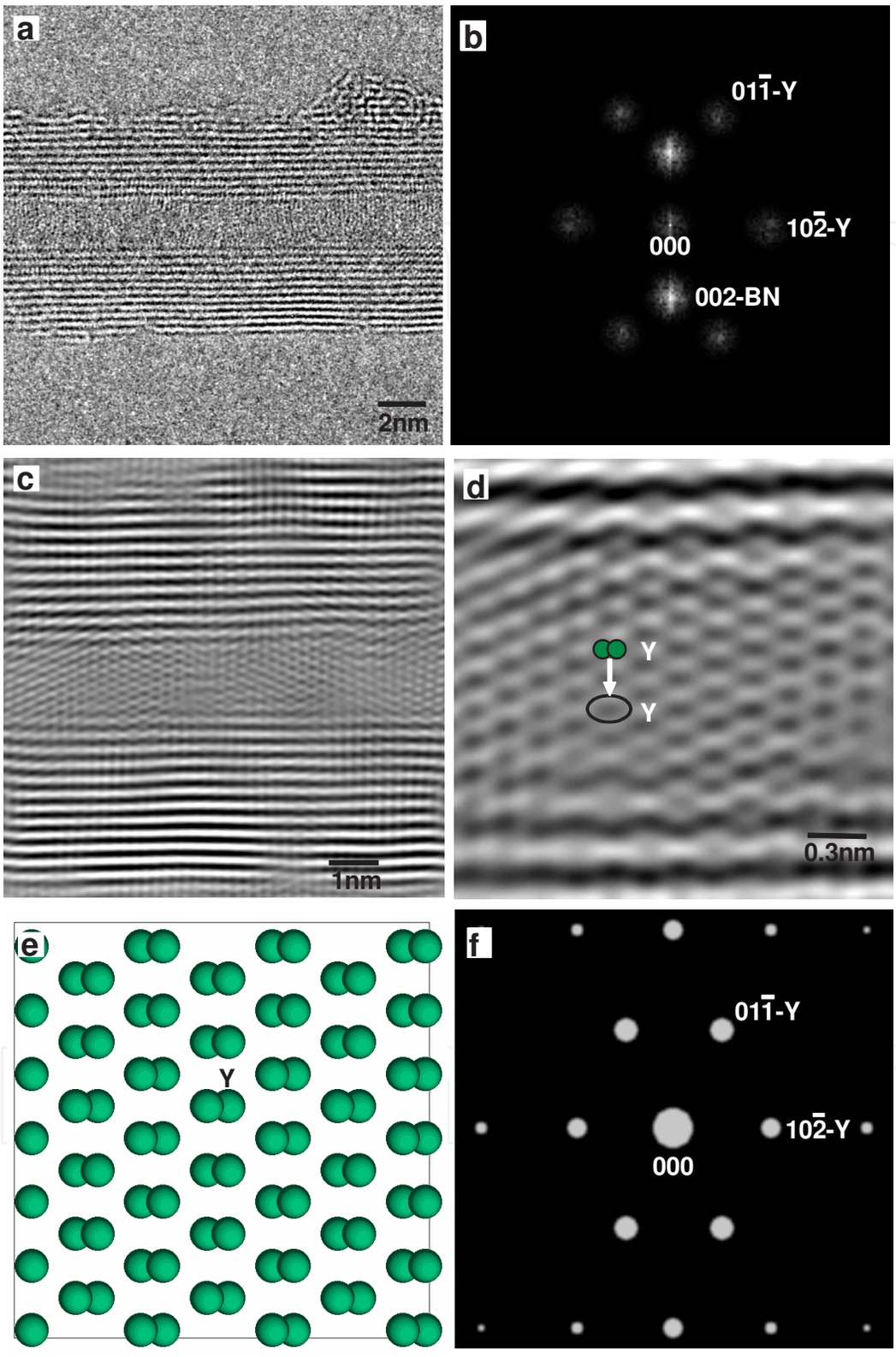

Figure 27. a) HREM image of BN nanotube synthesized from YB6 powder. (b) Filtered Fourier transform of (a). (c) Inverse Fourier transform of (b). (d) Enlarged image of (c). (e) Atomic structure model of yttrium along [101]. (f) Calculated diffraction pattern of (e).

http://dx.doi.org/10.5772/51968

A HREM image of a BN nanotube synthesized from YB_6 powder is also shown in Fig. 27(a), which was taken nearly at Scherzer defocus. Number of BN {002} layers is 12, and lattice fringes are observed in the BN nanotube. A filtered Fourier transform of Fig. 27(a) is shown in Fig. 27(b). Spots of BN 002 are observed as bright spots. In addition, reflections corresponding to the yttrium structure are observed and indexed with the incident electron beam along the [101] direction. Figure 27(c) is an inverse Fourier transform of Fig. 27(b), and BN{002} layers are clearly observed in the image. An enlarged image of Fig. 27(c) is shown in Fig. 27(d), which indicates lattice fringes at the center of the BN nanotube [91]. Lattice parameters of yttrium with a hexagonal structure, as determined by X-ray diffraction analysis, were a = 0.36474 nm and c = 0.57306 nm, which agrees well with the present lattice fringes (Oku et al. 2004). Dark contrast corresponds to yttrium atom pairs, as indicated in Fig. 27(d).

Based on the observations, an atomic structure model of yttrium along [101] was constructed as shown in Fig. 27(e), which indicates the yttrium atom pairs. Figure 27(f) is a calculated diffraction pattern of Fig. 27(e), and tense well with the observed Fourier transform of Fig. 27(b). Since YB_6 powders formed BN nanotubes in the present work, boron atoms were consumed preferentially. As a result, yttrium element would remain in the BN nanotube as a nanowire. These BN nanotubes with metal nanowires would be interesting nanomaterials for nanocables.

5. Conclusion

BN nanotubes with zigzag-, armchair-type and cup-stacked structures were synthesized and investigated by HREM, image simulation and total energy calculation. Hexagonal networks of BN nanotubes were directly observed by HREM in atomic scale, and chiralities of the BN nanotubes were directly determined from HREM images. Atomic structure models for quadruple- and double-walled nanotubes were proposed, and simulated images based on these models agreed well with experimental HREM images. Molecular mechanics calculations showed good stability of a zigzag-type structure compared to the armchair-type structure, which agreed well with the experimental data of disordered armchair-type BN nanotubes. BN nanotubes encapsulating a $B_{36}N_{36}$ cluster, and yttrium and Fe nanowires were also produced and confirmed by HREM and diffraction calculation.

Acknowledgments

The authors would like to acknowledge I. Narita, N. Koi, A. Nishiwaki, K. Suganuma, M. Inoue, K. Hiraga, M. Nishijima, R. V. Belosludov, and Y. Kawazoe for experimental help and useful advices.

Author details

Takeo Oku

The University of Shiga Prefecture, Japan

References

[1] Chopra, N., G., , Luyken, R. J., Cherrey, K., Crespi, V. H., Cohen, M. L., Louie, S. G., & Zettl, A. (1995). Boron nitride nanotubes. Science, , 269, 966-967.

[2] Endo, M., Kim, Y. A., Hayashi, T., Yanagisawa, T., Muramatsu, H., Ezaka, M., Terrones, H., Terrones, M., & Dresselhaus, M. S. (2003). Microstructural changes induced in "stacked cup" carbon nanofibers by heat treatment. Carbon, , 41, 1941-1947.

[3] Golberg, D., Bando, Y., Kurashima, K., & Sato, T. (2000). Ropes of BN multiwalled nanotubes. Solid State Communications, , 116, 1-6.

[4] Golberg, D., Xu, F. F., & Bando, Y. (2003). Filling boron nitride nanotubes with metals. Applied Physics A, , 76, 479-485.

[5] Ishigami, M., Sau, J. D., Aloni, S., Cohen, M. L., & Zettl, A. (2005). Observation of the giant stark effect in boron-nitride nanotubes. *Physical Review Letters*, 94, 056804-056801.

[6] Koi, N., Oku, T., Inoue, M., & Suganuma, K. (2008). Structures and purification of boron nitride nanotubes synthesized from boron-based powders with iron particles. *Journal of Materials Science*, 43, 2955-2961.

[7] Lauret, J. S., Arenal, R., Ducastelle, F., Loiseau, A., Cau, M., Attal-Tretout, B., Rosencher, E., & Goux-Capes, L. (2005). Optical transitions in single-wall boron nitride nanotubes. *Physical Review Letters*, 94, 037405-037401.

[8] Lim, S. H., Luo, J., Ji, W., & Lin, J. (2007). Synthesis of boron nitride nanotubes and its hydrogen uptake. Catalysis Today, , 120, 346-350.

[9] Mickelson, W., Aloni, S., Han, W. Q., Cumings, J., & Zettl, A. (2003). Packing C_{60} in boron nitride nanotubes. Science, , 300, 467-469.

[10] Narita, I., & Oku, T. (2003). Synthesis of boron nitride nanotubes by using NbB_2, YB_6 and YB_6/Ni powders. *Diamond and Related Materials*, 12, 1912-1917.

[11] Nishiwaki, A., Oku, T., Tokoro, H., & Fujii, S. (2005). Atomic structures and stability of boron nitride nanotubes with a cup-stacked structure. *Diamond and Related Materials*, 14, 1163-1168.

[12] Oku, T., & Narita, I. (2004). Atomic structures and stabilities of zigzag and armchair-type boron nitride nanotubes studied by high-resolution electron microscopy and molecular mechanics calculation. *Diamond and Related Materials*, 13, 1254-1260.

[13] Oku, T., Narita, I., Nishiwaki, A., & Koi, N. (2004). Atomic structures, electronic states and hydrogen storage of boron nitride nanocage clusters, nanotubes and nanohorns, Defects and Diffusion Forum, , 226-228, 113-141.

[14] Oku, T., Koi, N., Narita, I., Suganuma, K., & Nishijima, M. (2007). Formation and atomic structures of boron nitride nanotubes with cupstacked and Fe nanowire encapsulated structures. Materials Transactions, , 48, 722-729.

[15] Oku, T., Koi, N., & Suganuma, K. (2008). Electronic and optical properties of boron nitride nanotubes. Journal of Physics and Chemistry of Solids, , 69, 1228-1231.

[16] Oku, T., Narita, I., Koi, N., Nishiwaki, A., Suganuma, K., Inoue, M., Hiraga, K., Matsuda, T., Hirabayashi, M., Tokoro, H., Fujii, S., Gonda, M., Nishijima, M., Hirai, T., Belosludov, R. V., & Kawazoe, Y. (2009). Boron nitride nanocage clusters, nanotubes, nanohorns, nanoparticles, and nanocapsules, In: B-C-N nanotubes and related nanostructures. Y. K. Yap (Ed.), Springer., 149-194.

[17] Oku, T. (2011). High-resolution electron microscopy of nanostructured materials. Nanoscience & Nanotechnology-Asia, , 1, 59-75.

[18] Saito, Y., Okuda, M., Tomita, M., & Hayashi, T. (1995). Extrusion of single-wall carbon nanotubes via formation of small particles condensed near an arc evaporation source. Chemcal Physics Letters, , 236, 419-426.

[19] Radosavljevi, M., Appenzeller, J., Derycke, V. R., Ph, Avouris. M., Loiseau, A., Cochon, J., , L., & Pigache, D. (2003). Electrical properties and transport in boron nitride nanotubes. Applied Physics Letters, , 82, 4131-4133.

[20] Rubio, A., Corkill, J. L., & Cohen, M. L. (1994). Theory of graphitic boron nitride nanotubes. Physical Review B, , 49, 5081-5084.

[21] Tang, C. C., Bando, Y., & Sato, T. (2002). Synthesis and morphology of boron nitride nanotubes and nanohorns. Applied Physics A, , 75, 681-685.

[22] Wang, J., Kayastha, V. K., Yap, Y. K., Fan, Z., Lu, J. G., Pan, Z., Ivanov, I. N., Puretzky, A. A., & Geohegan, D. B. (2005). Low temperature growth of boron nitride nanotubes on substrates. *Nano letters*, 5, 2528-2532.

[23] Watanabe, K., Taniguchi, T., & Kanda, H. (2004). Direct-bandgap properties and evidence for ultraviolet lasing of hexagonal boron nitride single crystal. *Nature materials*, 3, 404-409.

[24] Wilder, J. W. G., Venema, L. C., Rinzler, A. G., Smalley, R. E., & Dekker, C. (1998). Electronic structure of atomically resolved carbon nanotubes. Nature, , 391, 59-62.

IntechOpen